Geochimica et Cosmochimica Acta 353 (2023) 112–128

Contents lists available at ScienceDirect

Geochimica et Cosmochimica Acta

journal homepage: www.elsevier.com/locate/gca

# Isotopic fractionation of chlorine and potassium during chloride sublimation under lunar conditions

Ziyan Han [a], Hejiu Hui [a,b,c,*], Haizhen Wei [a,b], Weiqiang Li [a,b]

[a] State Key Laboratory of Mineral Deposits Research, School of Earth Sciences and Engineering, Nanjing University, Nanjing 210023, China
[b] CAS Center for Excellence in Comparative Planetology, Hefei 230026, China
[c] CAS Key Laboratory of Earth and Planetary Physics, Institute of Geology and Geophysics, Chinese Academy of Sciences, Beijing 100029, China

ARTICLE INFO

*Associate editor:* James M.D. Day

*Keywords:*
Evaporation experiments
Cl isotopes
K isotopes
Metal chlorides
The Moon

ABSTRACT

The Moon is depleted in volatile elements and compounds, and lunar samples exhibit a wide range of Cl isotopic compositions, which is believed to result from the volatilization of metal chlorides (e.g., NaCl, KCl, and $FeCl_2$). However, the Cl isotopic fractionation behavior during volatilization is not well constrained, particularly for metal chlorides. Furthermore, the effect of metal chloride evaporation on metal isotopes is poorly known. In the present study, we performed NaCl and KCl sublimation experiments to study Cl and K isotopic fractionations at temperatures ranging from 923 K to 1061 K and at pressures of $7\times10^{-5}$ bar to 1 bar in an $N_2$ atmosphere. The isotope fractionation factors of $^{37/35}Cl(\alpha_{gas-solid})$ from NaCl sublimation experiments are 0.9985±0.0002, 0.9958 ±0.0004, and 0.99807±0.00004 at 1, $10^{-2}$, and $7\times10^{-5}$ bar, respectively. Those of $^{41/39}K(\alpha_{gas-solid})$ and $^{37/35}Cl$ $(\alpha_{gas-solid})$ from KCl sublimation experiments are 0.99884±0.00004 and 0.9988±0.0003 at 1 bar, 0.9977 ±0.0002 and 0.9972±0.0003 at $10^{-2}$ bar, and 0.9989±0.0002 and 0.9989±0.0001 at $7\times10^{-5}$ bar, respectively. Chlorine and K isotopes fractionate more at $10^{-2}$ bar than at $7\times10^{-5}$ bar and 1 bar. The saturation index in all the sublimation experiments was >95%, which resulted in near-equilibrium isotopic fractionation at the sublimation interface. Therefore, the isotopic fractionation was controlled by mass transfer processes in the gas and solid phases. The isotopic fractionation at $10^{-2}$ bar was controlled by the chemical diffusion of sublimated gas in an $N_2$ atmosphere with almost no convection effect, (i.e., *Pe* number close to zero), whereas the isotopic fractionation at 1 bar was suppressed by atmospheric convection with a turbulence factor of 0.4±0.1 (i.e., *Pe* number >1). The extremely high sublimation rate and the very slow diffusion in the sublimating solid at $7\times10^{-5}$ bar suppressed isotopic fractionations. Based on our experimental results, calculations using Cl/K and Na/K in lunar materials reveal that degassing of KCl contributed very little (<0.2‰) to the K isotopic fractionation (>0.58‰) during lunar magma ocean degassing. The Cl isotopic fractionation factor from lunar samples is similar to our results at $10^{-2}$ bar. This similarity of Cl isotope fractionation indicates that there may have been a transient atmosphere above the lunar magma ocean.

## 1. Introduction

The Moon is depleted in volatiles relative to Earth (O'Neill, 1991; Albarède et al., 2015). Furthermore, the moderately volatile elements with 50% condensation temperatures ($T_c$) that are ≤1290 K and ≥704 K (Palme et al., 1988; Lodders, 2003), such as K, Ga, Cu, Rb, Zn, and Cl, on the Moon are isotopically heavier than those of bulk silicate Earth (BSE) (e.g., Herzog et al., 2009; Sharp et al., 2010b; Paniello et al., 2012; Kato et al., 2015; Wang and Jacobsen, 2016; Pringle and Moynier, 2017; Nie and Dauphas, 2019; Tian et al., 2020; Wimpenny et al., 2022), except for Sn and Cr isotopes (Sossi et al., 2018; Wang et al., 2019). This depletion in moderately volatile elements combined with the isotope characteristics may be related to the giant impact formation event (Paniello et al., 2012; Wang and Jacobsen, 2016; Gargano et al., 2022), the outgassing of the lunar magma ocean (LMO) (Day and Moynier, 2014; Kato et al., 2015; Boyce et al., 2015; Dhaliwal et al., 2018; Sossi et al., 2018), and/or the degassing of mare basalt during eruption and cooling (Sharp et al., 2010b; Zhang, 2020; Ji et al., 2022).

Lunar samples exhibit the largest variation of $\delta^{37}Cl$ (~0‰ to 81‰ in general, relative to SMOC, standard mean ocean chloride) from all

* Corresponding author at: State Key Laboratory of Mineral Deposits Research, School of Earth Sciences and Engineering, Nanjing University, Nanjing 210023, China.
*E-mail address:* hhui@nju.edu.cn (H. Hui).

https://doi.org/10.1016/j.gca.2023.05.007
Received 9 August 2022; Accepted 8 May 2023
Available online 16 May 2023

available solar system materials (e.g., Sharp et al., 2013b; Boyce et al., 2015; Williams et al., 2016; Bellucci et al., 2017; Barrett et al., 2019; Gargano and Sharp., 2019; Wang et al., 2019; Hu et al., 2020). The large Cl isotopic fractionation in lunar samples is mainly thought to be a result of volatilization of metal chlorides (e.g., NaCl, KCl, $FeCl_2$, $ZnCl_2$) during magma eruption (Sharp et al., 2010b) and/or LMO solidification (Boyce et al., 2015; Barnes et al., 2016; Boyce et al., 2018; Barnes et al., 2019). The positive correlation between the $\delta^{37}Cl$ values of apatite and the KREEP (an abbreviation for K, rare-earth elements, and P) component in lunar basalts implies the incorporation of urKREEP, with the high $\delta^{37}Cl$ (~+25‰) resulting from degassing during LMO solidification (Boyce et al., 2015; Barnes et al., 2016; Boyce et al., 2018). However, this variation in $\delta^{37}Cl$ detected in lunar samples has also been interpreted to be a result of the mixing of multiple reservoirs or vapor-phase metasomatism (Potts et al., 2018; Barnes et al., 2019). The whole-rock $\delta^{37}Cl$ values of 16 Apollo basalts (7.3±3.5‰) are thought to have been caused by the depletion of halogens resulting from the giant impact formation of the Moon (Gargano et al., 2020). The 14.4‰ variation of Cl isotopes in the newly returned Chang'E-5 young basaltic fragments has been explained by the degassing and enrichment of chlorine-bearing species during magma crystallization (Ji et al., 2022).

Distinct from Cl isotopes, K isotopes display relatively limited variations in lunar basalts, with an average $\delta^{41}K$ (relative to NIST SRM 3141a) of –0.07±0.09‰, which is approximately 0.4‰ heavier than that in BSE (Wang and Jacobsen, 2016; Tian et al., 2020). This difference could have resulted from the high-energy Moon-forming giant impact (Wang and Jacobsen, 2016). Non-mare rocks on the Moon show slightly larger variations than mare basalts, with elevated $\delta^{41}K$ values of 0.23 ~0.51‰ in KREEP-rich breccias (Tian et al., 2020). The high $\delta^{41}K$ values of KREEP-rich materials could reflect the enrichment of heavy K isotopes in the urKREEP reservoir with similar heavy Cl isotopic enrichment resulting from KCl degassing during LMO solidification, whereas the light K isotopic compositions (as low as –2.60‰) in highland rocks could have resulted from condensation of light K isotope–rich vapors back to the lunar surface (Tian et al., 2020). In summary, the volatile evolution of the Moon remains under debate.

In silicate melts, the Cl degassing species can include HCl as well as different types of metal chlorides (e.g., NaCl, KCl, and $FeCl_2$), according to melt composition, $f_{O_2}$, $f_{Cl_2}$, temperature, pressure, and water content (Symonds and Reed, 1993; Ustunisik et al., 2015; Renggli et al., 2017; Scholtysik and Canil, 2021). Owing to the low $f_{O_2}$ on the Moon and the high diffusivity of $H_2$, $H_2$ is the main hydrogen species in vapor during magma degassing, and thus metal chlorides are the major Cl-degassing species on the Moon (Sharp et al., 2013a). Sodium, K, Zn, and Fe could evaporate from basaltic samples at >1273 K (De Maria et al., 1971; Sossi et al., 2019), which could bond with Cl during vaporization. The Zn-, S-, Na-, K-, and Cl-rich condensate coating on lunar pyroclastic glass beads (Butler and Meyer, 1976; McKay and Wentworth, 1993; Ma and Liu, 2019) indicates that the species of NaCl, KCl, and $ZnCl_2$ could be available in vapor. Thermodynamic calculations suggest that Zn prefers to evaporate as $Zn^0$ rather than as $ZnCl_2$ at 973–1773 K despite the preference for monoatomic gas over the chloride species for most metals at >1673 K (Renggli et al., 2017). Therefore, NaCl and KCl may be the two main species involved in Cl degassing on the Moon.

Kinetic effects could induce large isotopic fractionation during vaporization (Richter et al., 2002; Richter et al., 2011; Young et al., 2019; Sossi et al., 2020). Kinetic isotopic fractionation during vaporization can be affected by different processes, including vaporization at the interface and mass transfer in the melt and in the gas (e.g., Wang et al., 1999; Cappa, 2003; Yu et al., 2003; Richter et al., 2007; Richter et al., 2011; Sossi et al., 2020; Zhang et al., 2021; Young et al., 2022). To date, Cl isotope fractionation has only been investigated in the evaporation of hydrochloric acid solution ($\alpha_{gas-liquid}$ = 0.996) and hyperacid brines ($\alpha_{gas-liquid}$ = 0.9945–1.0030) at atmospheric pressure (Sharp et al., 2010a; Rodríguez et al., 2018). Therefore, a systematic understanding of Cl isotope fractionation during planetary vaporization remains lacking. By contrast, there are several reports of K isotope fractionation during vaporization as $K^0$ from silicate melt (Yu et al., 2003; Richter et al., 2011; Zhang et al., 2021; Neuman et al., 2022). However, the K isotope fractionation behavior when bonding with Cl has not been studied. Hence, experimentally quantifying the isotopic fractionation factors of different Cl-bearing species during degassing at varying pressures and temperatures is necessary for elucidating the volatile loss on the Moon.

Here, we conducted NaCl and KCl sublimation experiments at various temperatures and pressures in an $N_2$ atmosphere to investigate the reaction kinetics and isotope (Cl and K) fractionation behavior. We determined the Cl and K isotopic fractionation factors for NaCl and KCl at pressures ranging from $7\times10^{-5}$ bar to 1 bar. The objectives of this study were to examine the effects of pressure on isotopic behavior during vaporization and to determine the mechanism of isotopic fractionation during vaporization of Cl-bearing species in order to clarify the possible lunar atmospheric conditions when Cl isotopes were fractionated.

## 2. Theoretical framework

The evaporation theory is based on the kinetic theory of gases, the Hertz–Knudsen equation, and thermodynamics and has been described in detail in previous studies (Richter et al., 2002; Cappa, 2003; Sossi et al., 2020). A summary of this theoretical framework is presented here. According to the Hertz–Knudsen equation, the sublimation rate for a particular species $i$ through the surface over a given time interval is as follows (Hirth and Pound, 1963):

$$J_{sub} = -\frac{\Gamma_i\left(P_{i,sat} - P_i\right)}{\sqrt{2\pi M_i RT}}, \tag{1}$$

where $J_{sub}$ is the sublimation rate in $mol\cdot m^{-2}\cdot s^{-1}$, $\Gamma_i$ is the evaporation coefficient, $P_{i,sat}$ is the saturated vapor pressure in Pa, $P_i$ is the partial vapor pressure at the surface in Pa, $M_i$ is the molar mass in $kg\cdot mol^{-1}$, $R$ is the gas constant 8.31 $J\cdot mol^{-1}\cdot K^{-1}$, and $T$ is the temperature in K. The saturation index $S$ is defined as $\frac{P_i}{P_{i,sat}}$ (Richter et al., 2002), which turns Eq. (1) into the following:

$$J_{sub} = -\frac{\Gamma_i P_{i,sat}(1-S)}{\sqrt{2\pi M_i RT}}. \tag{2}$$

When $P_i$ is 0, the sublimation rate reaches the maximum value (i.e., free evaporation rate $J_{sat}$). The saturation index $S$ can be expressed with $J_{sat}$ and $J_{sub}$:

$$S = 1 - \frac{J_{sub}}{J_{sat}}. \tag{3}$$

The free evaporation rates of NaCl and KCl have been determined in sublimation experiments (Ewing and Stern, 1974).

Transport of the gas species away from the sublimation surface is controlled by mass transfer in the steady state, including diffusion and advection. The sublimation rate is thus equal to the mass transfer rate $J_{trans}$. The general form of mass transfer is described as follows:

$$J_{trans} = -\frac{h\left(P_i - P_{i,\infty}\right)}{RT}, \tag{4}$$

where $h$ is the mass transfer coefficient, and $P_{i,\infty}$ is the partial pressure of the species $i$ at an infinite distance from the evaporating surface. This partial pressure is zero in our experiments. The variable $P_i$ in the steady state could be calculated as $J_{sub} = J_{trans}$. The sublimation rate in the steady state is described as follows (Bartlett, 1967; Cappa, 2003; Sossi et al., 2020):

**Table 1**
Experimental conditions and results for NaCl sublimation.

| Sample | *P* (bar) | *T* (K) | Flow rate (SCCM) | Duration (h) | Initial mass (g) | Residual mass (g) | Corrected mass lost[d] (g) | *F* | $\delta^{37}Cl$[e] (‰) | $\Delta^{37}Cl_{ZT}$[f] (‰) |
|---|---|---|---|---|---|---|---|---|---|---|
| #A1[a] | 1 | 943 | 50 | 0 | 0.15035 | 0.14843 | 0.00000 | 1.00 | 0.46±0.50 (1) | 0.00 |
| #A2[a] | 1 | 943 | 50 | 110 | 0.15130 | 0.13753 | 0.01185 | 0.93 | 0.59±0.56 (2) | 0.14 |
| #A3[a] | 1 | 943 | 50 | 355.8 | 0.15046 | 0.10977 | 0.03878 | 0.75 | 0.76±0.69 (2) | 0.30 |
| #A4[a] | 1 | 943 | 50 | 669.7 | 0.15004 | 0.08494 | 0.06318 | 0.58 | 1.47±0.38 (2) | 1.02 |
| #A5[b] | 1 | 975 | 50 | 0 | 0.20003 | 0.19934 | 0.00000 | 1.00 | 0.45±0.30 (3) | 0.00 |
| #A6[b] | 1 | 975 | 50 | 40 | 0.20073 | 0.18896 | 0.01108 | 0.94 | 0.75±0.65 (3) | 0.29 |
| #A7[b] | 1 | 975 | 50 | 100 | 0.20046 | 0.17486 | 0.02492 | 0.88 | 0.87±0.67 (2) | 0.42 |
| #A8[b] | 1 | 975 | 50 | 150 | 0.20027 | 0.15811 | 0.04147 | 0.79 | 1.02±0.38 (2) | 0.57 |
| #A9[a] | 1 | 975 | 50 | 0 | 0.20043 | 0.19768 | 0.00000 | 1.00 | 0.38±0.25 (3) | 0.00 |
| #A10[a] | 1 | 975 | 50 | 40 | 0.20049 | 0.18727 | 0.01047 | 0.95 | 0.60±0.08 (2) | 0.22 |
| #A11[a] | 1 | 975 | 50 | 249 | 0.19973 | 0.12749 | 0.06949 | 0.65 | 0.96±0.24 (3) | 0.58 |
| #A12[a] | 1 | 975 | 50 | 374 | 0.20035 | 0.09467 | 0.10293 | 0.49 | 1.74±0.02 (2) | 1.36 |
| #A13[b] | 1 | 1010 | 50 | 0 | 0.40077 | 0.39950 | 0.00000 | 1.00 | 0.57±0.11 (2) | 0.00 |
| #A14[b] | 1 | 1010 | 50 | 10 | 0.39966 | 0.39030 | 0.00809 | 0.98 | 0.61±0.38 (1) | 0.04 |
| #A15[b,g] | 1 | 1010 | 50 | 30 | 0.39944 | 0.37481 | 0.02336 | 0.94 | 0.73±0.43 (4) | 0.15 |
| #A16[b,g] | 1 | 1010 | 50 | 30 | 0.39976 | 0.37664 | 0.02185 | 0.95 | 0.51±0.15 (3) | –0.07 |
| #A17[b] | 1 | 1010 | 50 | 60 | 0.40069 | 0.35343 | 0.04598 | 0.89 | 1.10±0.27 (2) | 0.53 |
| #A18[b] | 1 | 1010 | 50 | 120 | 0.24996 | 0.16223 | 0.08647 | 0.65 | 1.20±0.04 (3) | 0.63 |
| #A19[b] | 1 | 1010 | 50 | 120 | 0.40001 | 0.30808 | 0.09066 | 0.77 | 0.97±0.38 (3) | 0.40 |
| #A20[b] | 1 | 1006 | 50 | 150 | 0.19986 | 0.10689 | 0.09170 | 0.54 | 1.49±0.53 (3) | 0.92 |
| #A21[a] | 1 | 1010 | 50 | 0 | 0.40064 | 0.39718 | 0.00000 | 1.00 | 0.80±0.14 (2) | 0.00 |
| #A22[a] | 1 | 1010 | 50 | 60 | 0.40062 | 0.35176 | 0.04540 | 0.89 | 1.03±0.10 (2) | 0.23 |
| #A23[a] | 1 | 1010 | 50 | 184 | 0.20178 | 0.06639 | 0.13193 | 0.34 | 2.22±0.37 (4) | 1.42 |
| #A24[b] | 1 | 1061 | 50 | 0 | 0.40055 | 0.39827 | 0.00000 | 1.00 | 0.72±0.42 (4) | 0.00 |
| #A25[b,h] | 1 | 1061 | 50 | 5 | 0.39969 | 0.38239 | 0.01503 | 0.96 | 0.73±0.42 (1) | 0.00 |
| #A26[b,h] | 1 | 1061 | 50 | 5 | 0.39996 | 0.38294 | 0.01474 | 0.96 | 0.54±0.39 (1) | –0.19 |
| #A27[b] | 1 | 1061 | 50 | 10 | 0.39996 | 0.36780 | 0.02988 | 0.93 | 0.84±0.38 (1) | 0.12 |
| #A28[b,i] | 1 | 1061 | 50 | 20 | 0.39956 | 0.34014 | 0.05715 | 0.86 | 1.13±0.19 (3) | 0.40 |
| #A29[b,i] | 1 | 1061 | 50 | 20 | 0.39968 | 0.34089 | 0.05651 | 0.86 | 0.76±0.06 (2) | 0.04 |
| #A30[b] | 1 | 1057 | 50 | 20 | 0.39980 | 0.34878 | 0.04875 | 0.88 | 0.70±0.28 (4) | –0.02 |
| #A31[b,i] | 1 | 1061 | 50 | 20 | 0.40046 | 0.33897 | 0.05921 | 0.85 | 0.79±0.17 (2) | 0.07 |
| #A32[b] | 1 | 1061 | 50 | 40 | 0.39956 | 0.28139 | 0.11590 | 0.71 | 1.18±0.25 (3) | 0.46 |
| #A33[b] | 1 | 1061 | 50 | 80 | 0.39873 | 0.16615 | 0.23031 | 0.42 | 1.39±0.16 (3) | 0.67 |
| #A34[b] | 1 | 1057 | 50 | 100 | 0.40050 | 0.14897 | 0.24925 | 0.38 | 1.83±0.46 (2) | 1.11 |
| #A35[b] | 1 | 1057 | 50 | 110 | 0.40038 | 0.13935 | 0.25876 | 0.35 | 2.06±0.26 (3) | 1.33 |
| #A36[b] | 1 | 1061 | 50 | 120 | 0.40026 | 0.06300 | 0.33499 | 0.16 | 2.86±0.53 (4) | 2.13 |
| #A37[b] | 1 | 1061 | 50 | 120 | 0.79968 | 0.46250 | 0.33491 | 0.58 | 1.60±0.35 (3) | 0.88 |
| #A38[a] | 1 | 1061 | 50 | 0 | 0.39966 | 0.39781 | 0.00000 | 1.00 | 0.43±0.55 (2) | 0.00 |
| #A39[a] | 1 | 1061 | 50 | 20 | 0.39981 | 0.33794 | 0.05960 | 0.85 | 0.87±0.09 (2) | 0.44 |
| #A40[a] | 1 | 1061 | 50 | 40 | 0.39944 | 0.27333 | 0.12384 | 0.69 | 1.00±0.23 (2) | 0.57 |
| #A41[b] | 1 | 1061 | 200 | 0 | 0.40069 | 0.39574 | 0.00000 | 1.00 | 0.54±0.58 (2) | 0.00 |
| #A42[b] | 1 | 1061 | 200 | 20 | 0.39971 | 0.28353 | 0.11123 | 0.72 | 1.03±0.36 (1) | 0.49 |
| #A43[b] | 1 | 1061 | 200 | 40 | 0.39969 | 0.17499 | 0.21974 | 0.45 | 1.41±0.07 (2) | 0.87 |
| #A44[a] | 1 | 1061 | 200 | 60 | 0.39997 | 0.09669 | 0.29833 | 0.25 | 4.00±0.36 (5) | 3.46 |
| | | | | | | | | | | |
| #B45[c] | $10^{-2}$ | 974 | 0 | 6 | 0.40060 | 0.33122 | 0.06318 | 0.84 | 1.41±0.24 (3) | 0.62 |
| #B46[c] | $10^{-2}$ | 974 | 0 | 11.78 | 0.40092 | 0.25316 | 0.14157 | 0.65 | 3.03±0.23 (3) | 2.24 |
| #B47[c] | $10^{-2}$ | 974 | 0 | 23.5 | 0.40075 | 0.14952 | 0.24503 | 0.39 | 4.57±0.27 (4) | 3.78 |
| #B48[c] | $10^{-2}$ | 974 | 0 | 19.42 | 0.40121 | 0.18914 | 0.20587 | 0.49 | 4.04±0.15 (3) | 3.26 |
| #B49[c] | $10^{-2}$ | 974 | 0 | 0 | 0.39981 | 0.39361 | 0.00000 | 1.00 | 0.79±0.31 (3) | 0.00 |
| | | | | | | | | | | |
| #C50[c] | $7\times10^{-5}$ | 923 | 0 | 0 | 0.39982 | 0.39384 | 0.00000 | 1.00 | 0.77±0.29 (3) | 0.00 |
| #C51[c,j] | $7\times10^{-5}$ | 923 | 0 | 0.83 | 0.39998 | 0.27098 | 0.12302 | 0.69 | 1.40±0.34 (2) | 0.63 |
| #C52[c,j] | $7\times10^{-5}$ | 923 | 0 | 0.83 | 0.39982 | 0.27865 | 0.11519 | 0.71 | 1.41±0.18 (3) | 0.63 |
| #C53[c] | $7\times10^{-5}$ | 923 | 0 | 1.7 | 0.40006 | 0.14964 | 0.24444 | 0.39 | 2.59±0.33 (2) | 1.82 |
| #C54[c] | $7\times10^{-5}$ | 923 | 0 | 2 | 0.40041 | 0.11727 | 0.27716 | 0.31 | 3.01±0.23 (3) | 2.23 |
| #C55[c] | $7\times10^{-5}$ | 974 | 0 | 0.25 | 0.20091 | 0.04978 | 0.12815 | 0.25 | 3.53±0.81 (2) | 2.75 |
| #C56[c] | $7\times10^{-5}$ | 974 | 0 | 0.5 | 0.39988 | 0.09274 | 0.28417 | 0.29 | 3.07±0.46 (4) | 2.29 |
| #C57[c] | $7\times10^{-5}$ | 974 | 0 | 0 | 2.00054 | 1.97756 | 0.00000 | 1.00 | 0.67±0.42 (3) | 0.00 |
| #C58[c] | $7\times10^{-5}$ | 974 | 0 | 0.5 | 2.00031 | 1.70523 | 0.27210 | 0.86 | 0.98±0.08 (3) | 0.31 |
| #C59[c,k] | $7\times10^{-5}$ | 974 | 0 | 1 | 2.00035 | 1.38030 | 0.59707 | 0.70 | 1.23±0.37 (5) | 0.55 |
| #C60[c,k] | $7\times10^{-5}$ | 974 | 0 | 1 | 2.00070 | 1.39254 | 0.58518 | 0.71 | 1.24±0.31 (4) | 0.56 |
| #C61[c] | $7\times10^{-5}$ | 974 | 0 | 2 | 2.00019 | 0.82780 | 1.14941 | 0.43 | 1.53±0.38 (1) | 0.85 |
| #C62[c] | $7\times10^{-5}$ | 974 | 0 | 3 | 2.00026 | 0.29761 | 1.67967 | 0.16 | 1.67±0.04 (3) | 1.00 |

[g,h,i,j,k] These are duplicate experiments.

[a] Sample heating in this experiment was started and stopped at the target temperature.

[b] The sample in this experiment was heated from room temperature (about 20 °C) to the target temperature over 2 h. After heating, the sample was cooled from the target temperature to 373 K over 4 h and was then removed from the furnace.

[c] The sample was heated to the target temperature and 1 bar for ~10 min to reach thermal equilibrium, and then the sample chamber was pumped to the target pressure over ~2 min. After heating, the vacuum pump connection to the sample chamber was closed, and air was slowly injected into the sample chamber until the pressure reached 1 bar in ~2 min. The sample crucible was removed from the furnace at the target temperature and 1 bar.

[d] The corrected mass loss is the mass sublimated in the experiment relative to that in the zero-time experiment.
[e] The number between the parentheses is the number of the isotope measurement.
[f] ZT denotes the deviation (‰) relative to the products of the zero-time experiments.

$$J_{sub} = -\frac{\frac{\Gamma_i P_{i,sat}}{\sqrt{2\pi R M_i T}}}{1 + \frac{\Gamma_i RT}{h\sqrt{2\pi R M_i T}}}. \quad (5)$$

Combining Eqs. (2) and (5), the saturation index $S$ can be determined:

$$S = 1 - \frac{1}{1 + \frac{\Gamma_i RT}{h\sqrt{2\pi R M_i T}}}. \quad (6)$$

When $h$ is large, $S$ tends to approach 0. However, when $h$ is small, $S$ is close to 1, and the sublimation rate can be determined using Eq. (4) with $P_i = P_{i,sat}$. The saturation index $S$ is controlled by the ratio of the mass transfer coefficient $h$ to the thermal velocity $\sqrt{\frac{2RT}{M_i}}$ of the species $i$ (Charnoz et al., 2021; Young et al., 2022).

The isotopic fractionation coefficient between gas and solid ($\alpha_{\text{gas–solid}}$) is the sublimation rate ratio of the two isotope species:

$$\alpha_{\text{gas–solid}} = \frac{J_{sub,2}}{J_{sub,1}} = \frac{\alpha_{eq}\alpha_{sub}\alpha_{tran}}{(1-S)\alpha_{tran} + S\alpha_{sub}}, \quad (7)$$

where $\alpha_{eq}$ is the equilibrium isotopic fractionation factor; $\alpha_{sub}$, equal to $\frac{\Gamma_{i2}}{\Gamma_{i1}}\sqrt{\frac{M_1}{M_2}}$, is the kinetic isotopic fractionation factor at the sublimation surface (Richter et al., 2002); and $\alpha_{tran}$, equal to $h_2/h_1$, is the kinetic isotopic fractionation induced by the chemical diffusion in the gas (Cappa, 2003; Sossi et al., 2020). When $h$ is large, $\alpha_{\text{gas–solid}}$ is $\alpha_{eq}\frac{\Gamma_{i2}}{\Gamma_{i1}}\sqrt{\frac{M_1}{M_2}}$. However, when $h$ is small, $\alpha_{\text{gas–solid}}$ becomes

$$\alpha_{\text{gas–solid}} = \alpha_{eq}\frac{h_2}{h_1}. \quad (8)$$

The mass transfer includes the chemical diffusion and convection resulting from eddy diffusion and thermal diffusion. If the mass transfer is dominated by chemical diffusion, $h$ can be expressed as the following:

$$h = \frac{D_{i,gas}}{L}, \quad (9)$$

where $D_{i,gas}$ is the chemical diffusivity in $m^2 \cdot s^{-1}$, and $L$ is the characteristic diffusion length in m. If the mass transfer is controlled by both diffusion and convection, $h$ depends on the aerodynamic conditions (Jacobson et al., 2020). The mass transfer coefficient ratio can be calculated approximately (Stewart, 1975):

**Table 2**
Experimental conditions and results for KCl sublimation.

| Sample | $P$ (bar) | $T$ (K) | Flow rate (SCCM) | Duration (h) | Initial mass (g) | Residual mass (g) | Corrected mass loss[d] (g) | $F$ | $\delta^{37}Cl$[e] (‰) | $\Delta^{37}Cl^{f}_{ZT}$ (‰) | $\delta^{39}K$[e] (‰) | $\Delta^{39}K^{f}_{ZT}$ (‰) |
|---|---|---|---|---|---|---|---|---|---|---|---|---|
| #A63[b] | 1 | 1020 | 50 | 0 | 0.39920 | 0.39700 | 0.00000 | 1.00 | –0.61±0.22 (3) | 0.00 | 0.24±0.08 (4) | 0.00 |
| #A64[b] | 1 | 1020 | 50 | 5 | 0.40015 | 0.38664 | 0.01132 | 0.97 | –0.66±0.38 (4) | –0.04 | 0.28±0.07 (3) | 0.04 |
| #A65[b] | 1 | 1020 | 50 | 10 | 0.39907 | 0.37417 | 0.02269 | 0.94 | –0.77±0.15 (2) | –0.16 | 0.28±0.10 (3) | 0.04 |
| #A66[a] | 1 | 993 | 50 | 45.80 | 0.20172 | 0.14712 | 0.05261 | 0.74 | –0.49±0.12 (3) | 0.15 | 0.57±0.04 (4) | 0.38 |
| #A67[a] | 1 | 993 | 50 | 78.12 | 0.19963 | 0.10771 | 0.08995 | 0.55 | 0.32±0.36 (4) | 0.93 | 0.90±0.09 (3) | 0.71 |
| #A68[a] | 1 | 993 | 50 | 0 | 0.19990 | 0.19792 | 0.00000 | 1.00 | –0.64±0.28 (3) | –0.03 | 0.19±0.13 (4) | 0.00 |
| #A69[a] | 1 | 993 | 50 | 119.70 | 0.19993 | 0.05465 | 0.14330 | 0.28 | 1.05±0.22 (4) | 1.67 | 1.61±0.10 (3) | 1.42 |
| #B70[c] | $10^{-2}$ | 945 | 0 | 17.87 | 0.39955 | 0.20142 | 0.19523 | 0.51 | 1.55±0.42 (5) | 2.14 | 2.02±0.04 (3) | 1.78 |
| #B71[c] | $10^{-2}$ | 945 | 0 | 27.13 | 0.40066 | 0.06060 | 0.33717 | 0.16 | 4.03±0.28 (8) | 4.61 | 4.07±0.09 (4) | 3.82 |
| #B72[c] | $10^{-2}$ | 945 | 0 | 8.13 | 0.40004 | 0.30699 | 0.09016 | 0.77 | –0.25±0.31 (3) | 0.33 | 0.96±0.10 (4) | 0.71 |
| #B73[c] | $10^{-2}$ | 945 | 0 | 0 | 0.40011 | 0.39722 | 0.00000 | 1.00 | –0.59±0.36 (3) | 0.00 | 0.25±0.10 (4) | 0.00 |
| #B74[c] | $10^{-2}$ | 945 | 0 | 22.30 | 0.40049 | 0.09003 | 0.30757 | 0.23 | 3.74±0.17 (8) | 4.33 | 3.48±0.07 (4) | 3.23 |
| #C75[c,g] | $7\times10^{-5}$ | 945 | 0 | 0.17 | 0.39992 | 0.27752 | 0.10455 | 0.74 | –0.19±0.11 (3) | 0.36 | 0.76±0.09 (3) | 0.49 |
| #C76[c,g] | $7\times10^{-5}$ | 945 | 0 | 0.17 | 0.40108 | 0.26337 | 0.11986 | 0.70 | –0.2±0.15 (3) | 0.35 | 0.73±0.06 (3) | 0.45 |
| #C77[c] | $7\times10^{-5}$ | 945 | 0 | 0 | 0.39975 | 0.38189 | 0.00000 | 1.00 | –0.55±0.39 (4) | 0.00 | 0.27±0.09 (3) | 0.00 |
| #C78[c] | $7\times10^{-5}$ | 945 | 0 | 0.33 | 0.39975 | 0.15659 | 0.22531 | 0.44 | 0.22±0.37 (3) | 0.76 | 1.29±0.10 (3) | 1.02 |
| #C79[c] | $7\times10^{-5}$ | 945 | 0 | 0.42 | 0.40009 | 0.11735 | 0.26489 | 0.34 | 0.66±0.38 (4) | 1.20 | 1.27±0.08 (4) | 1.00 |
| #C80[c] | $7\times10^{-5}$ | 945 | 0 | 0.25 | 0.39969 | 0.21121 | 0.17063 | 0.57 | 0.25±0.33 (3) | 0.80 | 0.87±0.05 (4) | 0.60 |

[a,b,c,d,e,f,g] Refer to the notes in Table 1.

$$\alpha_{tran} \approx \left(\frac{D_{2,gas}}{D_{1,\ gas}}\right)^{n}, \tag{10}$$

where $n$ is the turbulence factor, a parameter ranging from 0 (completely turbulent diffusion) to 1 (chemical diffusion) (Cappa, 2003). The turbulence factor $n$ depends on the aerodynamic conditions above the evaporation surface (Gonfiantini et al., 2018). The ratio of chemical diffusivity can be calculated using the kinetic theory of gases (Chapman and Cowling, 1970):

$$\frac{D_{2,gas}}{D_{1,gas}} = \left(\frac{M_1(M_2+M_g)}{M_2(M_1+M_g)}\right)^{\frac{1}{2}}, \tag{11}$$

where $M_g$ is the molar mass of the gas medium. In the present study, we performed sublimation experiments at different pressures to investigate the effects of pressure on $S$, $n$, and the isotopic fractionation factors.

## 3. Method

### 3.1. Sublimation experiments

A simple system with well-studied kinetics during free evaporation is ideal for investigation of pressure and aerodynamic effects on kinetic isotopic fractionation. We used NaCl and KCl powders (99.99%, Shanghai Aladdin Biochemical Technology Co., Ltd.) as the starting materials for our sublimation experiments. Approximately 30 g of powder was ground in an agate mortar for ≥30 min until the grain sizes were <200 mesh for NaCl and KCl, respectively. The ground powders were then stored in a desiccator for the high-temperature experiments.

For the sublimation experiments, 150–2000 mg of NaCl or KCl powder was precisely weighed, with a precision better than 0.1 mg. The weighed samples were placed into a corundum crucible (46 mm × 17 mm × 14 mm) for each experiment, ensuring that the salt powder was spread evenly in the crucible. The sublimation experiments were conducted at pressures of $7\times10^{-5}$ bar, $10^{-2}$ bar, and 1 bar and at different temperatures (923 K to 1061 K) in two split horizontal quartz tube furnaces (OTF-1200X, Kejing Company) with continuous flux of $N_2$ at the State Key Laboratory for Mineral Deposits Research, Nanjing University. All experiments were performed at temperatures below the melting points of NaCl (1074 K) and KCl (1043 K). An S-type thermocouple was used to determine temperature after calibration using the melting points of pure silver (99.99%) and pure gold (99.99%). The temperature uncertainty during the measurements was less than ±2 K. The flow rate of $N_2$ was held constant at ~50 standard cubic centimeters per minute (SCCM) and at 200 SCCM using a gas supply system (GSL-32, Kejing company) for the 1-bar experiments. The pressure was controlled using a vacuum pressure regulating system (GZK-PID-VRD24, Kejing company) for the low-pressure experiments, and the flow rate was held below 0.5 SCCM to maintain a nitrogen atmosphere. All running conditions are shown in Tables 1 and 2. The samples in experiments performed at 1 bar, $10^{-2}$ bar, and $7\times10^{-5}$ bar are referred to as "A," "B," and "C," respectively (Tables 1 and 2). Zero-time (ZT) experiments were performed at each running condition to correct for the effects of temperature, pressure, flow rate, and heating routine on sublimation rate and isotope fractionation. The corrected experimental durations were subsequently determined (Tables 1 and 2). After each sublimation experiment, the crucible was placed in a desiccator to cool down to room temperature (about 20 °C). The cooled crucible with the sample was weighed again to determine the mass loss during sublimation. The evaporation residue particles and the corundum crucible were carefully checked to ensure that the crucible did not react with NaCl or KCl during evaporation. All of the powder in the crucible was then dissolved in MilliQ water (18.2 MΩ·cm$^{-1}$). These solutions, with known NaCl or KCl contents, were used for isotope measurements.

Similar methods have been used to determine the Mg, Fe, Si, Cu, Zn, K, Te, Cr, and Tl isotopic fractionation factors during evaporation (e.g., Richter et al., 2002; Dauphas et al., 2004; Richter et al., 2011; Mendybaev et al., 2013; Sossi et al., 2020; Renggli et al., 2022; Neuman et al., 2022; Klemme et al., 2022). In all these experiments, the evaporation residues were analyzed to obtain high-quality isotopic fractionation factors. The condensations from evaporation products were not collected in most literature studies because any loss of the evaporation products can easily lead to an incorrect fractionation factor. On the other hand, thermogravimetric apparatus and mass spectrometers have been used to obtain high-quality thermodynamic data for NaCl or KCl sublimation (e.g., Miller and Kusch, 1956; Berkowitz and Chupka, 1958; Rothberg et al., 1959; Lester and Somorjai, 1968; Ewing and Stern, 1973; Wagoner and Hirth, 1977). However, the aim of this study is not to determine the thermodynamic data but to determine the isotopic fractionation factors of Cl and K during sublimation of metal chlorides at different pressures. Therefore, the weighing method with mass precision better than 0.1 mg is sufficient to study the isotopic fractionation factors of Cl and K during evaporation.

### 3.2. Chlorine isotopic analyses

The chlorine isotopic compositions of products from the sublimation experiments were analyzed using a Triton TI mass spectrometer (Thermo Fisher Finnigan, Germany) at the State Key Laboratory for Mineral Deposits Research, Nanjing University. The Cl-bearing solution was first passed through a 0.5-mL H-form resin column and then through a 0.5-mL Cs-form resin column following the procedure reported by Xiao et al. (1992). This two-column ion-exchange procedure converted the Cl-bearing solution into a CsCl solution, which was loaded onto the mass spectrometry filaments. A brief summary of Cl isotope measurement is presented here, and the detailed procedure has been described by Wei et al. (2012). Tantalum filaments (99.995%; 7.5 mm × 0.76 mm × 0.025 mm) were degassed for 1 h with a 3.0 A current under vacuum and were then oxidized for ≥24 h in the ambient atmosphere before use. Approximately 0.5 μL slurry of pure graphite (John-Matthew Company, 99.9999% pure) mixed with an 80% ethanol/20% water (v/v) solution was loaded on the center of each filament. Sample solution with 4–10 μg of chlorine in the form of CsCl was then loaded onto the filament. The sample on the filament was dried with a 0.2 A current to eliminate any possible loss of Cl. During the isotopic analyses, the filament current was increased to 1000 mA for 10 min and to ~ 1100 mA at a rate of 10 mA·min$^{-1}$ for stable emission of $Cs_2Cl^+$ ion. Data acquisition began when the $^{133}Cs_2^{35}Cl^+$ ($m/z$ = 301) ion beam reached ~1.0 V. The chlorine isotope ratio was obtained on the mass to charge ratio of 303 to 301 ($^{133}Cs_2^{37}Cl^+/^{133}Cs_2^{35}Cl^+$) for 6 analytical blocks of 10 cycles (6 blocks × 10 cycles).

The $\delta^{37}$Cl values were calculated according to the following equation:

$$\delta^{37}\mathrm{Cl}(‰) = \left[\frac{\left(\frac{^{37}\mathrm{Cl}}{^{35}\mathrm{Cl}}\right)_{\mathrm{sample}}}{\left(\frac{^{37}\mathrm{Cl}}{^{35}\mathrm{Cl}}\right)_{\mathrm{SMOC}}} - 1\right] \times 1000. \tag{12}$$

The $\delta^{37}$Cl data are reported relative to SMOC with a defined value of 0‰. In this study, we used a reference material (ISL 354 NaCl) from the International Atomic Energy Agency (IAEA) as the chlorine isotope standard of SMOC. The average value of $(^{37}Cl/^{35}Cl)_{SMOC}$ measured during our analyses was 0.318935 ± 0.000134 (2SD, $N$=25), which is consistent with the value 0.318898 ± 0.000174 (2SD, $N$=6), obtained using a Triton TI reported by Wei et al. (2012). Another reference material, NIST SRM 975 (isotopic chlorine) was analyzed during the isotope measurements. The average $\delta^{37}$Cl of 0.46 ± 0.36‰ (2SD, $N$=33) that we obtained for NIST SRM 975 is consistent with the value of 0.43‰ reported in the literature (Xiao et al., 2002).

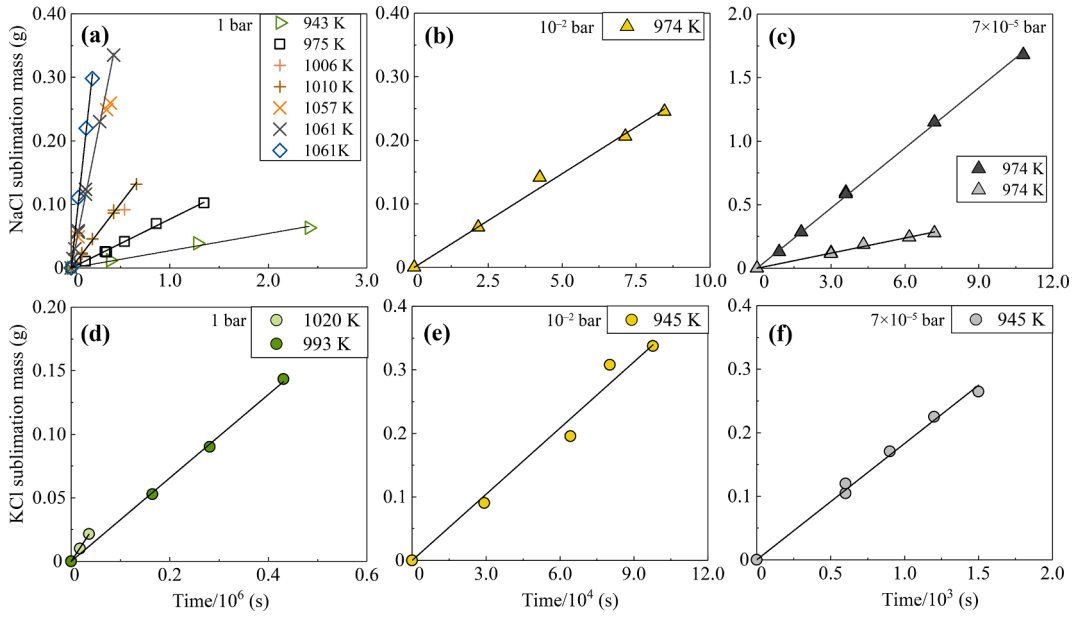


**Fig. 1.** Mass sublimated as a function of time for NaCl at (a) 1 bar, (b) $10^{-2}$ bar, and (c) $7\times10^{-5}$ bar, and for KCl at (d) 1 bar, (e) $10^{-2}$ bar, and (f) $7\times10^{-5}$ bar. The experiments at 1 bar were performed at a flow rate of 50 SCCM, except for those marked with diamonds in (a), which were performed at a flow rate of 200 SCCM. The sublimation rate at each temperature is constant through time.

### 3.3. Potassium isotopic analyses

The potassium isotopic compositions of the products of the sublimation experiments were analyzed using a Nu 1700 Sapphire High-Resolution Multiple-Collector Inductively Coupled Plasma Mass Spectrometer (HR-MC-ICP-MS) at the State Key Laboratory for Mineral Deposits Research, Nanjing University. An aliquot of dissolved sample containing 75–200 μg of K was dried and re-dissolved repeatedly in 100 μL concentrated $HNO_3$. The sample was then dried and dissolved in 2% $HNO_3$ in preparation for the isotopic analyses. The concentrations of K in the $HNO_3$ solution were measured using a flame photometer. High-precision K isotope analysis has been described in detail by An et al. (2022). A dry and hot plasma setting was used for the K isotope measurements. A large $^{40}Ar^+$ beam was neutralized through the ion guide rail (deflector) for a Daly detector. The interference of $^{40}ArH^+$ on $^{41}K^+$ was eliminated using the high-resolution mode of the instrument ($M/\Delta M > 15000$). Isotope ratios of K are expressed in delta notation:

$$\delta^{41}K(‰) = \left[\frac{\left(\frac{^{41}K}{^{39}K}\right)_{sample}}{\left(\frac{^{41}K}{^{39}K}\right)_{NIST3141a}} - 1\right] \times 1000. \quad (13)$$

The $\delta^{41}K$ data are reported relative to NIST SRM 3141a. The typical internal precision of a single analytical run was better than ± 0.04‰, and the external reproducibility was better than ±0.1‰ (2SD) (An et al., 2022).

## 4. Results

### 4.1. Sublimation rates

A total of 80 experiments (62 for NaCl and 18 for KCl) were performed at temperatures ranging from 923 K to 1061 K and at pressures of $7\times10^{-5}$ bar, $10^{-2}$ bar, and 1 bar (Tables 1 and 2). All samples

**Table 3**
Sublimation rates and isotope fractionation factors under different conditions.

| Sample | $T$ (K) | $P$ (bar) | Flow rate (SCCM) | $J_{sub}$ (mol·m$^{-2}$·s$^{-1}$) | $J_{sat}$ (mol·m$^{-2}$·s$^{-1}$)[a] | $S$ | $^{37/35}Cl(\alpha_{gas-solid})$ | $^{41/39}K(\alpha_{gas-solid})$ | $D_{i,gas}$ (cm$^2$·s$^{-1}$) | $Pe$ |
|---|---|---|---|---|---|---|---|---|---|---|
| NaCl | 1061 | 1 | 50 | $1.67\times10^{-5}$ | 1.030 | 0.999984 | | | 1.45 | 1.46 |
| NaCl | 1061 | 1 | 200 | $3.02\times10^{-5}$ | 1.030 | 0.999971 | | | 1.45 | 5.86 |
| NaCl | 1010 | 1 | 50 | $4.33\times10^{-6}$ | 0.254 | 0.999983 | | | 1.34 | 1.59 |
| NaCl | 975 | 1 | 50 | $1.64\times10^{-6}$ | 0.095 | 0.999983 | | | 1.26 | 1.68 |
| NaCl | 943 | 1 | 50 | $5.80\times10^{-7}$ | 0.036 | 0.999984 | | | 1.19 | 1.78 |
| NaCl | | 1 | | | | | 0.9985±0.0002 | | | |
| NaCl | 974 | $10^{-2}$ | 0 | $6.30\times10^{-5}$ | 0.092 | 0.999317 | 0.9958±0.0004 | | $1.26\times10^{2}$ | $1.69\times10^{-4}$ |
| NaCl | 974 | $7\times10^{-5}$ | 0 | $3.36\times10^{-3}$ | 0.092 | 0.963597 | | | $1.91\times10^{4}$ | $7.30\times10^{-9}$ |
| NaCl | 923 | $7\times10^{-5}$ | 0 | $8.48\times10^{-4}$ | 0.019 | 0.955833 | | | $1.75\times10^{4}$ | $7.98\times10^{-9}$ |
| NaCl | | $7\times10^{-5}$ | | | | | 0.99807±0.00004[b] | | | |
| KCl | 1020 | 1 | 50 | $9.89\times10^{-6}$ | 0.666 | 0.999985 | | | 1.31 | 1.62 |
| KCl | 993 | 1 | 50 | $5.51\times10^{-6}$ | 0.308 | 0.999982 | | | 1.26 | 1.68 |
| KCl | | 1 | | | | | 0.9988±0.0003 | 0.99884±0.00004 | | |
| KCl | 945 | $10^{-2}$ | 0 | $5.83\times10^{-5}$ | 0.075 | 0.999223 | 0.9972±0.0003 | 0.9977±0.0002 | $1.17\times10^{2}$ | $1.81\times10^{-4}$ |
| KCl | 945 | $7\times10^{-5}$ | 0 | $3.07\times10^{-3}$ | 0.075 | 0.959067 | 0.9989±0.0001 | 0.9989±0.0002 | $1.78\times10^{4}$ | $7.84\times10^{-9}$ |

[a] Data are from Ewing and Stern (1974).
[b] Samples with initial masses of 2 g were not included in the calculations.

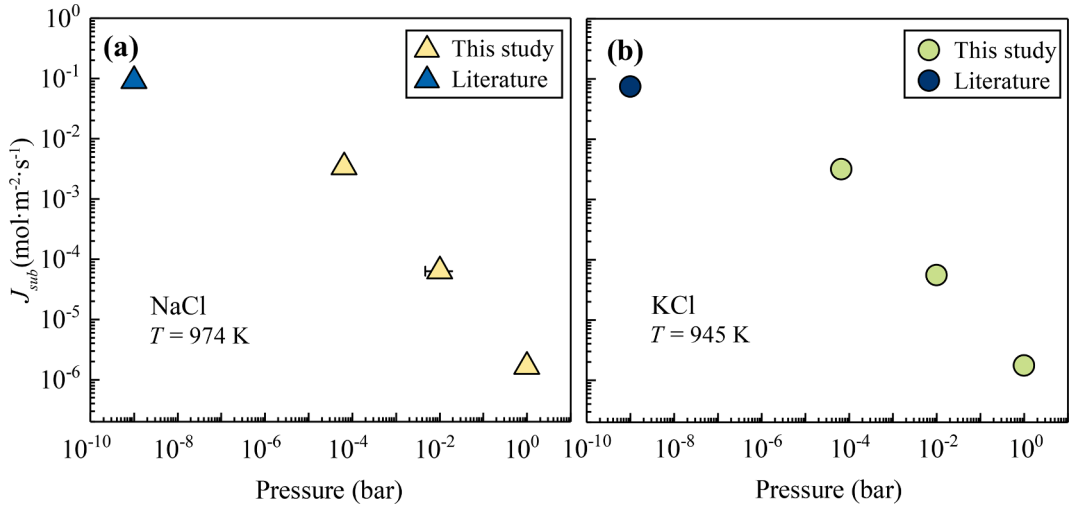


**Fig. 2.** Correlation between sublimation rate $J_{sub}$ and pressure for (a) NaCl at 974 K and (b) KCl at 945 K. The sublimation rate of KCl at 1 bar and 945 K was extrapolated from the results of 993 K and 1020 K at 1 bar. The free evaporation experimental data for NaCl and KCl are from the literature (Ewing and Stern, 1974).

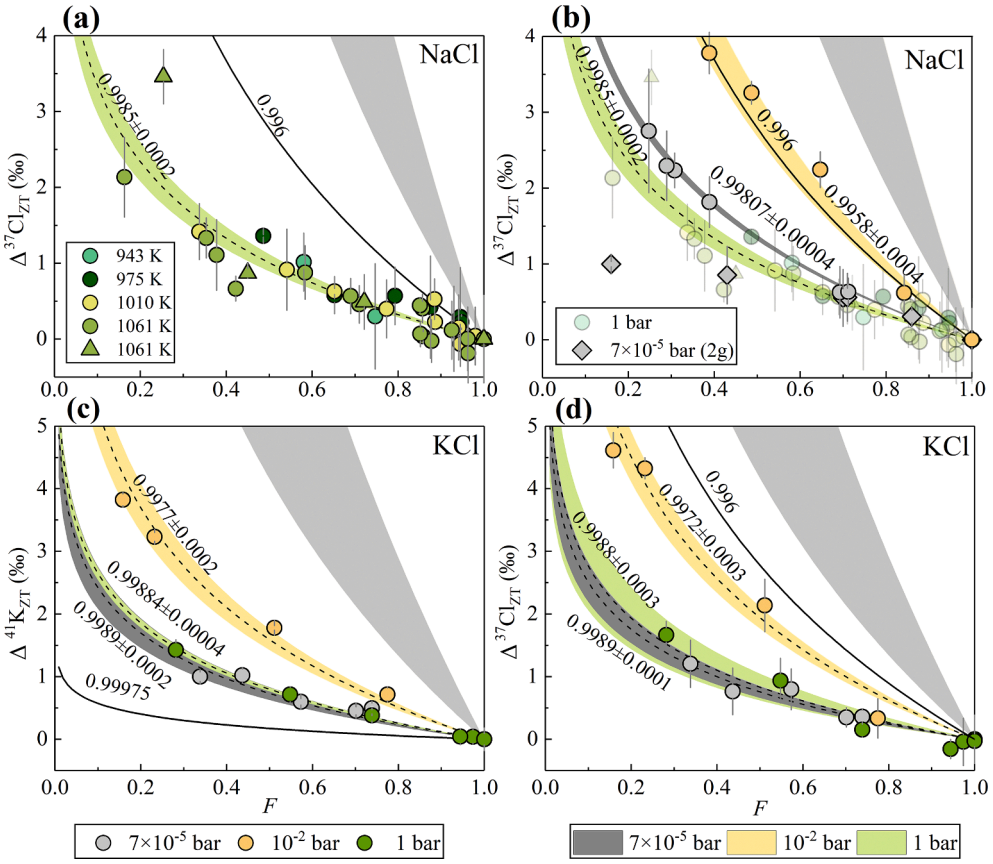


**Fig. 3.** Correlation between the isotopic composition and the mass fraction of residues after sublimation experiments with NaCl and KCl. The experiments at 1 bar were performed with a flow rate of 50 SCCM, except those marked with triangles in (a), which were performed with a flow rate of 200 SCCM. All uncertainties and error envelopes represent 2 standard deviations (SD). The dashed lines are fits of the data using Eq. (14). Data from samples with an initial mass of 2 g were not included in the regression. The light gray areas represent the isotopic fractionation factors of NaCl and KCl free evaporation, which were calculated using $\sqrt{M_1/M_2}$. The solid curves represent the Cl and K isotopic fractionation factors of Apollo samples (Wang and Jacobsen, 2016; Boyce et al., 2018; Tian et al., 2020).

experienced mass loss during sublimation with a maximum value of 85.1% (Tables 1 and 2). The sublimated masses of NaCl and KCl were linear with time and were independent of the initial sample weight (Fig. 1), consistent with results reported for previous experiments (Zimm and Mayer, 1944; Lester and Somorjai, 1968; Wagoner and Hirth, 1977; Sata, 1992). Except for the NaCl experiments at 1006 K and 1057 K, which may have been affected by temperature fluctuations (up to 4 K), the sublimation rate at each temperature–pressure–flow rate condition was determined using the linear correlation between sublimation mass and heating time (Table 3; Fig. 1). The sublimation rate increased as the temperature or the flow rate increased (Fig. 1a and 1d). By contrast, the sublimation rate was negatively correlated with pressure (Fig. 2). The sublimation rate at $7\times10^{-5}$ bar was >1000 times greater than that at 1 bar at the same temperature.

### 4.2. Potassium and chlorine isotopic fractionation during sublimation

The potassium and chlorine isotope results presented here are relative to their zero-time (ZT) experimental results ($\Delta^{41}K_{ZT}$ and $\Delta^{37}Cl_{ZT}$, respectively) and are summarized in Tables 1 and 2. Several duplicate

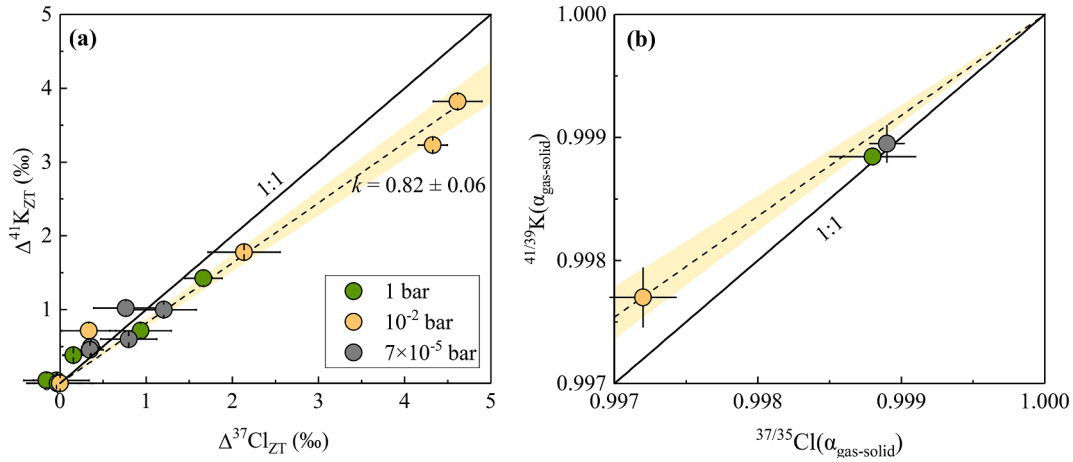


**Fig. 4.** Correlations between (a) $\Delta^{37}Cl_{ZT}$ and $\Delta^{41}K_{ZT}$ and between (b) $^{37/35}Cl(\alpha_{gas-solid})$ and $^{41/39}K(\alpha_{gas-solid})$ in the KCl sublimation experiments. The dashed line in (a) represents the linear fit of the data, and the shadowed area represents the uncertainty (2SD). The dashed line and shadowed area in (b) were calculated using the correlation between Cl and K isotopic fractionations in (a).

experiments were performed to ensure the reproducibility of our experimental results. The Cl and K isotopic fractionations of the duplicate experiments were indistinguishable within the analytical errors (Tables 1 and 2). The $\Delta^{37}Cl_{ZT}$ values of the NaCl sublimation residues ranged from –0.19±0.39‰ to 3.78±0.27‰ (Table 1). The $\Delta^{37}Cl_{ZT}$ values of the KCl sublimation residues ranged from –0.16±0.15‰ to 4.61±0.28‰, and their $\Delta^{41}K_{ZT}$ values varied from 0.00±0.08‰ to 3.82 ±0.09‰ (Table 2). The chlorine isotopic fractionation was slightly greater than the potassium isotopic fractionation in the same sublimation residual sample.

The isotope fractionation correlated positively with the residual mass fraction (Fig. 3). Except for the results from the experiments with an initial weight of 2 g, the K and Cl isotope fractionation factors between gas and solid during sublimation can be described using the Rayleigh distillation fractionation model:

$$\delta_f - \delta_0 = (1000 + \delta_0) \times \left(F^{(\alpha_{gas-solid}-1)} - 1\right) \quad (14)$$

where $\delta_f$ is the isotopic composition of the sublimation residual relative to its zero-time experimental result, $\delta_0$ is the isotopic composition of the corresponding zero-time experimental sample (defined as 0‰), $\alpha_{gas-solid}$ is the isotopic fractionation factor, and $F$ is the mass fraction of the residual after the experiment. The correlation between the chlorine isotopic fractionation and the residual mass fractions from all 1-bar experiments yielded a constant isotopic fractionation factor (Fig. 3a). However, the Cl isotopic fractionation factor changed with changes in experimental pressure (Fig. 3b). During NaCl sublimation, the calculated $^{37/35}Cl(\alpha_{gas-solid})$ was 0.9985±0.0002 at 1 bar, 0.9958±0.0004 at

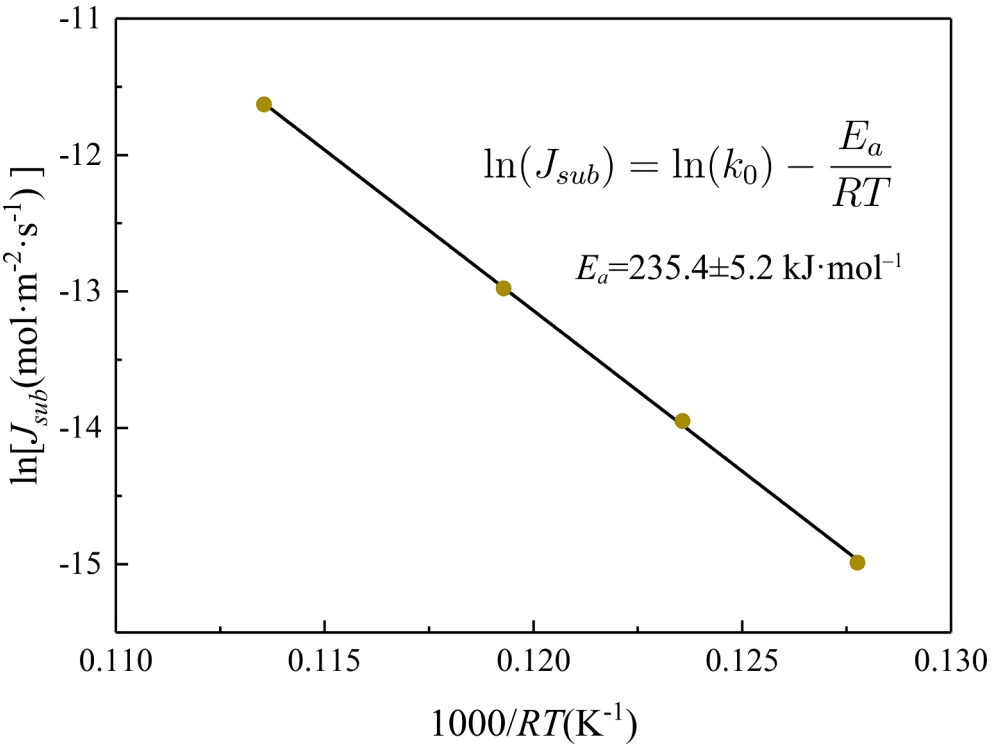


**Fig. 5.** Arrhenius equation for NaCl sublimation at 1 bar. The apparent activation energy is 235.4±5.2 kJ·mol$^{-1}$, which is between those of NaCl (220.8 kJ·mol$^{-1}$) and $Na_2Cl_2$ (245.3 kJ·mol$^{-1}$) (Lester and Somorjai, 1968).

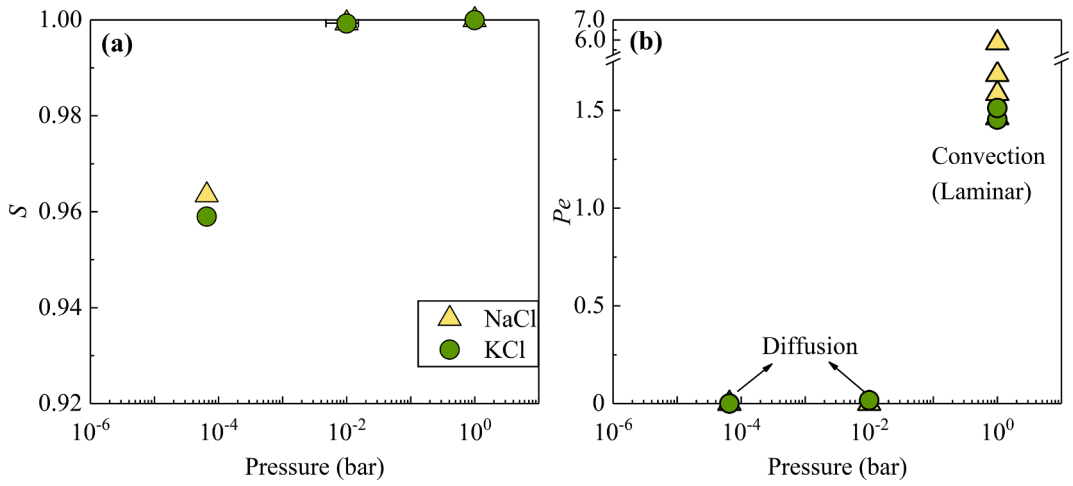


**Fig. 6.** Pressure effects on (a) the saturation index and (b) the Péclet number.

$10^{-2}$ bar, and 0.99807±0.00004 at $7\times10^{-5}$ bar. Similarly, during KCl sublimation, the calculated $^{37/35}Cl(\alpha_{gas-solid})$ was 0.9988±0.0003 at 1 bar, 0.9972±0.0003 at $10^{-2}$ bar, and 0.9989±0.0001 at $7\times10^{-5}$ bar. In these KCl sublimation experiments, the calculated $^{41/39}K(\alpha_{gas-solid})$ was 0.99884±0.00004 at 1 bar, 0.9977±0.0002 at $10^{-2}$ bar, and 0.9989 ±0.0002 at $7\times10^{-5}$ bar. The isotopic fractionation factors at $10^{-2}$ bar were higher than those at either 1 bar or $7\times10^{-5}$ bar for both NaCl and KCl. The potassium and chlorine isotopic fractionation factors were the same in the KCl sublimation experiments at 1 bar and at $7\times10^{-5}$ bar, whereas the $^{37/35}Cl(\alpha_{gas-solid})$ was slightly smaller than the $^{41/39}K$ $(\alpha_{gas-solid})$ at $10^{-2}$ bar (Fig. 4b; Table 3).

## 5. Discussion

### 5.1. Speciation and kinetics of sublimation

Experiments have shown that the species of NaCl and KCl during vaporization are mainly monomer and dimer with very few trimers (e.g., Rothberg et al., 1959; Milne and Klein, 1960; Lester and Somorjai, 1968; Butman et al., 2000). The proportion of dimer increases with increasing temperature, and the ratio of dimer to monomer may vary depending on the properties of the evaporation surface (Butman et al., 2000). Different stoichiometries of sodium chloride such as $NaCl_3$ and $Na_3Cl$ have been detected at high pressure (Zhang et al., 2013). However, these unexpected stoichiometries of sodium chloride are unstable at low pressure. Therefore, only the monomeric and dimeric forms of NaCl and KCl have been considered in this study.

The effect of temperature on the sublimation kinetics can be quantitatively described using the apparent activation energy in the Arrhenius Equation:

$$J_{sub} = k_0 e^{-\frac{E_a}{RT}}, \tag{14}$$

where $k_0$ is the pre-exponential factor and $E_a$ is the apparent activation energy in kJ·mol$^{-1}$. The apparent activation energy and the pre-exponential factor of NaCl sublimation at 1 bar were determined to be 235.4±5.2 kJ·mol$^{-1}$ and $3.6\times10^6$ mol·m$^{-2}$·s$^{-1}$, respectively (Fig. 5). This apparent activation energy value is between those of the monomer (220.8 kJ·mol$^{-1}$) and the dimer (245.3 kJ·mol$^{-1}$) during NaCl evaporation (Lester and Somorjai, 1968), indicating that both species could exist in the vapor during sublimation.

The sublimation rates of NaCl at 974 K and KCl at 945 K increase substantially with decreasing pressure (Fig. 2), indicating a decrease of the saturation index of NaCl and KCl according to Eq. (2). The partial pressure of the evaporating species was not measured to obtain the saturation index during evaporation in the literature (e.g., Richter et al., 2011; Gonfiantini et al., 2018; Sossi et al., 2020; Neuman et al., 2022). On the other hand, the saturation index can be calculated using Eq. (3) with the free evaporation rate $J_{sat}$ determined at each temperature (Ewing and Stern, 1974). The sublimation rates of NaCl and KCl in all our experiments were >25 times lower than those in the free evaporation experiments at high vacuum (<$10^{-9}$ bar) (Ewing and Stern, 1974). The value of $S$ decreased from 99.9984 % to 95.5833 % with decreasing pressure (Table 3; Fig. 6a), consistent with the concept that chemical diffusivity in the gas media increases with decreasing pressure (diffusivity itself is proportional to $1/P$; Chapman and Cowling, 1970).

Equation (4) indicates that the sublimation rate is affected by the mass transfer coefficient $h$. The mass transfer coefficient depends on the transport conditions of gas (Jacobson et al., 2020). Our experimental conditions can be simplified as chloride sublimation from a flat plate to the flowing gas or static gas media. The Péclet number $Pe$ (Table 3; Fig. 6b) is used to evaluate the relative importance between convection and chemical diffusion in gas transport and is expressed as follows:

$$Pe = \frac{UL}{D_{i,gas}}, \tag{15}$$

where $U$ is the media gas ($N_2$ in the present study) velocity in m·s$^{-1}$, $L$ is the characteristic length in m (0.5 m, half the length of the furnace tube in the present study), and $D_{i,gas}$ is the chemical diffusivity of the sublimated species $i$ in m$^2$·s$^{-1}$.

This chemical diffusivity can be calculated using the Chapman-Enskog relation (Chapman and Cowling, 1970). The large gas diffusivity and extremely low flow rate in the experiments performed at pressures < 1 bar result in $Pe$ values of nearly zero (Table 3; Fig. 6b). The aerodynamic conditions in these experiments were similar to those of static gas, in which diffusion in gas is dominant in mass transfer: that is to say, mass transfer coefficient $h$ equals $D_{i,gas}/L$ in Eq. (9). By contrast, $Pe$ in the 1-bar experiments is slightly>1, indicating that convection and advection play an important role in mass transfer. It is difficult to determine the mass transfer coefficient in these 1-bar experiments.

### 5.2. Mechanism of Cl isotope fractionation during NaCl sublimation

The isotopic fractionation between gas and solid during sublimation is controlled by the equilibrium isotope fractionation and the kinetic isotope fractionation. The latter results from sublimation at the interface and transport in the gas and the solid. Equilibrium isotopic fractionation is negligible at high temperatures. Density Functional Theory (DFT) calculations have shown that the equilibrium isotopic fractionation factor between gaseous NaCl and crystalline NaCl at 923 K is >0.999968 (Balan et al., 2019). Therefore, in this study, the kinetic isotope

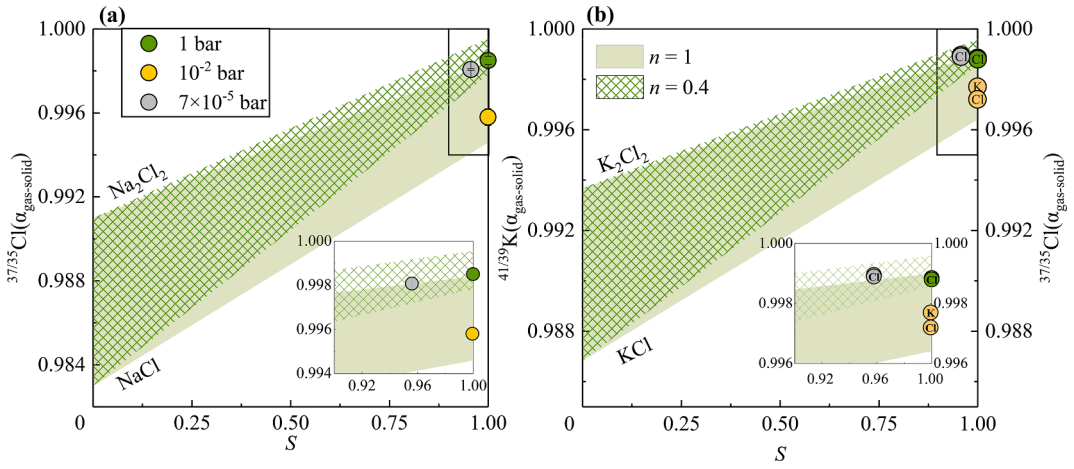


**Fig. 7.** The isotopic fractionation factor as a function of saturation index for (a) NaCl and (b) KCl. The upper boundary of each closed shadowed area represents the $\alpha_{gas-solid}$ of the dimer, and the lower boundary represents that of the monomer. The green shadowed areas were calculated using Eqs. (7) and (10) with turbulence factors of 0.4 for the cross-hatched pattern and 1 for the solid pattern, respectively. The isotopic fractionations for both NaCl and KCl at 1 bar were consistent with mass transfer with turbulence factor of 0.4, whereas those at $10^{-2}$ bar were consistent with diffusion in static gas. The isotopic fractionations at $7\times10^{-5}$ bar were suppressed by diffusion in the residues (see text for discussion).

fractionation effect was much more important than equilibrium isotopic fractionation during NaCl sublimation as shown in Eq. (7). The relative contributions of sublimation at the interface and diffusion in the gas to isotopic fractionation are determined by the saturation index *S*. The values of *S* can be obtained by comparing the evaporation rates in our experiments and in vacuum using Eq. (3) (see Section 5.1). The values of *S* were >95% in all our experiments (Table 3). In the evaporation experiments with the *S* values close to 1 (Fig. 6a), the contribution of kinetic isotope fractionation at the sublimation interface to the observed isotope fractionation was very small as shown in Eq. (7). On the other hand, the influence of the diffusive isotope fractionation in the solid depends on the timescale difference between diffusion in the solid and sublimation of the solid. In the present study, we focused on the influence of mass transfer processes in the gas and in the solid on isotopic fractionation.

*5.2.1. Aerodynamic influence on isotopic fractionation in the gas phase*

Previous studies have measured diffusive isotopic fractionation in gas through evaporation experiments at 1 bar, including H and O isotopes in water (e.g., Craig et al., 1963; Stewart, 1975; Merlivat, 1978; Cappa, 2003; Luz et al., 2009; Gonfiantini et al., 2018), and K, Zn, Cu, Tl, and Cr in silicate melts (Yu et al., 2003; Richter et al., 2011; Sossi et al., 2020; Nielsen et al., 2021; Klemme et al., 2022; Neuman et al., 2022). In general, diffusive isotopic fractionation factors deviated from theoretical values obtained using Eq. (11). In other words, the turbulence factor *n* in Eq. (10) is much less than unity and is controlled by the aerodynamic conditions above the evaporation interface, including the flow rate, the thermal gradient above the evaporation interface, and the roughness of the interface (Horita et al., 2008; Gonfiantini et al., 2018). The turbulence factor approaches one when convection and advection are not responsible for mass transfer in the gas. Water evaporation experiments showed that most turbulence factors are < 0.5 in flow stream, and that turbulence factors range from 0.7 to 1 in relatively static gas (Gonfiantini et al., 2018). Aerodynamic effects on the turbulence factor at high temperatures have been discussed rarely. Sossi et al. (2020) proposed the *n* value to be 2/3 in laminar regime on the basis of the mass transfer coefficient being proportional to the $D_{i,gas}^{2/3}$ based on the Chilton-Colburn analogy. This *n* value could explain the observed Cu, Zn, K, Tl, and Cr isotope fractionation factors in 1-bar evaporation experiments from different studies (Yu et al., 2003; Richter et al., 2011; Sossi et al., 2020; Nielsen et al., 2021; Klemme et al., 2022; Neuman et al., 2022).

The aerodynamics in our experiments could not be directly measured. However, the relative contribution of chemical diffusion in gas mass transfer could be assessed using the *Pe* number (Table 3; Fig. 6b). The *Pe* values were close to 0 in the <1-bar experiments; thus, the turbulence factor *n* in these experiments can be assumed to be 1. Moreover, the gas flowing in 1-bar experiments with *Pe* >1 can contribute to the mass transfer via advection, and thus *n* is <1. This hypothesis is consistent with the observation of greater Cl isotope fractionation in NaCl sublimation in experiments performed at $10^{-2}$ bar than those performed at 1 bar, i.e., the fractionation factor is closer to 1 when *n* deviates from unity as shown in Eq. (10). The $^{37/35}Cl(\alpha_{gas-solid})$ value (0.9958±0.0004) measured during NaCl sublimation at $10^{-2}$ bar is between the theoretical $^{37/35}Cl(\alpha_{gas-solid})$ values of NaCl monomer (0.9946) and NaCl dimer (0.9984) in $N_2$ determined using Eq. (11) (Fig. 7a), implying that *n* is equal or close to 1 under the $10^{-2}$ bar conditions. By contrast, the $^{37/35}Cl(\alpha_{gas-solid})$ value (0.9985±0.0002) measured in the 1-bar experiments is greater than the theoretical value of NaCl dimer. Thermodynamic calculations at temperatures of ~923 K to 1061 K (Chase 1998) indicate that the dimer could not be the dominant species under the experimental conditions in this study, implying that *n* is <1 under the 1-bar conditions.

The proportion of dimer in the sublimated gas was determined using the mixing proportion of the two gas species in the measured apparent isotopic fractionation factor at $10^{-2}$ bar (see Supplementary Materials Section S1). In the present study, the dimer molar ratio for NaCl was estimated to be $20^{+8}_{-7}$ % at 974 K. This molar ratio is within the reported dimer ratio range of 12–40 % reported by various authors who used mass spectrometry or gravimetric methods (Miller and Kusch, 1956; Berkowitz and Chupka, 1958; Rothberg et al., 1959; Lester and Somorjai, 1968; Wagoner and Hirth, 1977; Kvande et al., 1979; Butman et al., 2000) and the thermodynamic calculation (28%, see Supplementary Materials Section S1; Chase 1998). The dimer ratio could be affected by difference of the evaporation coefficient $\Gamma_i$ for these two species as shown in Eq. (1). The evaporation coefficient is typically less than unity during the sublimation of solid (e.g., Hashimoto, 1990; Davis et al. 1990, Richter et al. 2002), but cannot be determined in our experiments. On the other hand, the dimer ratios measured in the previous studies have included effect of evaporation coefficient difference between monomer and dimer (Miller and Kusch, 1956; Berkowitz and Chupka, 1958; Rothberg et al., 1959; Lester and Somorjai, 1968; Butman et al., 2000). The dimer ratios determined in our experiments include the effect of evaporation coefficient. Nevertheless, dimer ratios determined in our experiments are in line with the published data despite

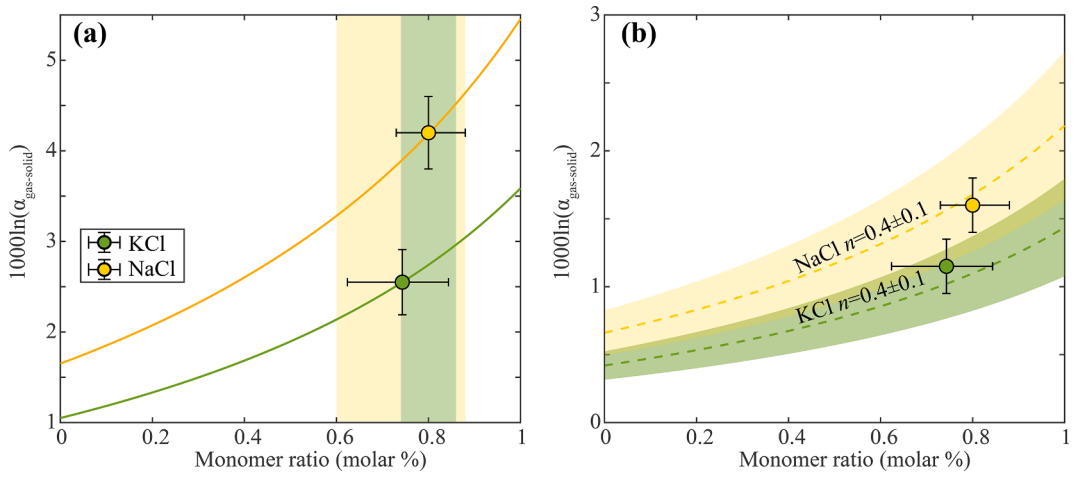


**Fig. 8.** Isotopic fractionation factor as a function of monomer ratio of NaCl and KCl at (a) $10^{-2}$ bar and (b) 1 bar. The yellow area and the green area in (a) represent the monomer ratio ranges of NaCl and KCl from literature data (Miller and Kusch, 1956; Berkowitz and Chupka, 1958; Rothberg et al., 1959; Lester and Somorjai, 1968; Wagoner and Hirth, 1977; Kvande et al., 1979; Chase, 1998; Butman et al., 2000), respectively. The solid lines in (a) are the theoretical curves of 1000ln ($\alpha_{gas–solid}$) as a function of monomer ratio. The dashed lines and associated areas in (b) are the theoretical curves of the isotopic fractionation factor with turbulence factor $n = 0.4\pm0.1$.

pressure differences (Fig. 8a), confirming that $n$ is close to 1 and that chemical diffusion is dominant in mass transfer at $10^{-2}$ bar.

The dimer ratio of NaCl and the apparent isotope fractionation factor were used to estimate the turbulence factor at 1 bar. This estimation yielded values for $n$ ranging from 0.3 to 0.5 with the best value being 0.4 (Fig. 8b). This best value is comparable to those determined in water evaporation experiments in flow stream (Craig et al., 1963; Cappa, 2003; Gonfiantini et al., 2018), but it differs from the $n$ value of 2/3 obtained in silicate evaporation experiments (Sossi et al., 2020). This difference may have been caused by variable aerodynamic conditions in the evaporation experiments (e.g., sample shape, furnace tube size, gas flow rate, pressure, thermal gradient). Above all, aerodynamics likely plays a key role in isotopic fractionation in gas.

### 5.2.2. *Diffusion-limited evaporation of solid*

The NaCl evaporation experiments reveal that the Cl isotopic fractionation factor between gas and solid at $7\times10^{-5}$ bar is much lower than that at $10^{-2}$ bar. The smaller *Pe* numbers at $7\times10^{-5}$ bar compared to those at $10^{-2}$ bar and 1 bar (Table 3; Fig. 6b) indicate that diffusion is much more critical than convection for mass transfer in the gas at $7\times10^{-5}$ bar. In contrast to the experiments performed at 1 bar, convection in the gas could not result in the smaller isotopic fractionations observed at $7\times10^{-5}$ bar. Furthermore, the relatively smaller $S$ value of 96% at $7\times10^{-5}$ bar (Table 3) should have led to larger isotopic fractionation if the solid phase was isotopically homogeneous. Therefore, the solid phase at $7\times10^{-5}$ bar may not have been isotopically homogeneous during sublimation. Analogously, the Cl isotopic fractionation in evaporation experiments with an initial weight of 2 g may have differed from the Cl isotopic fractionation in experiments with lower initial weights (Fig. 3b). The isotopic fractionation in the evaporation experiments with lower initial weights followed the Rayleigh distillation model. The suppression of Cl isotopic fractionation in the $7\times10^{-5}$-bar experiments may have resulted from the diffusion-limited sublimation of solid.

Isotope fractionation during diffusion-limited evaporation, in which the sublimation rate is much larger than the isotope homogenization

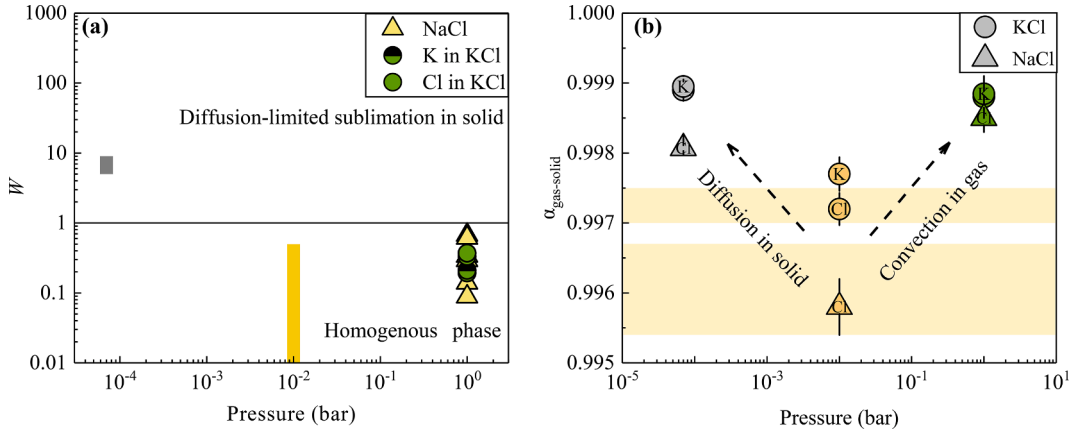


**Fig. 9.** (a) Correlation between $W$ (ratio of the diffusion and the sublimation timescales) and pressure. The gray and yellow bars represent the $W$ range for experiments at $7\times10^{-5}$ and $10^{-2}$ bar determined numerically using Eq. (S10), respectively. The solid triangles and circles represent the $W$ for experiments at 1 bar calculated using Eq. (S8). The sublimating solid in experiments at 1 bar and $10^{-2}$ bar, in which $W < 1$, was homogenous, whereas the isotopic fractionation in experiments at $7\times10^{-5}$ bar, in which $W=7\pm2$, was affected by diffusion in the solid. (b) Correlation between the isotopic fractionation factors of Cl and K during NaCl and KCl sublimation and pressure. The yellow bands represent the theoretical diffusive isotopic fractionation factors of gas-phase NaCl and KCl. The $\alpha_{gas–solid}$ values at 1 bar were influenced by gas convection in the experiments with $n=0.4\pm0.1$. Diffusion-limited sublimation of solid led to the $\alpha_{gas–solid}$ at $7\times10^{-5}$ bar being larger than that at $10^{-2}$ bar.

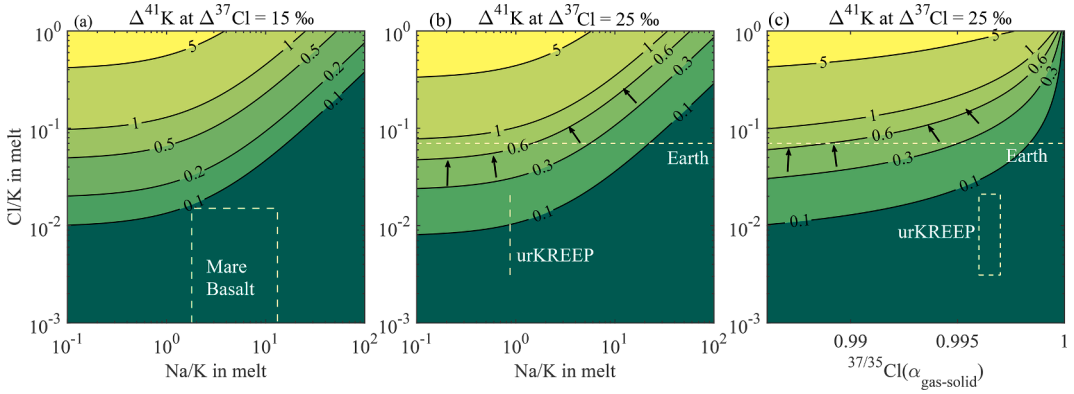


**Fig. 10.** Contribution of KCl degassing to K isotopic fractionation in (a) mare basalt with $\Delta^{37}$Cl of 15‰, (b) urKREEP with $\Delta^{37}$Cl of 25‰ (Boyce et al., 2018) and isotopic fractionation factor of 0.983 for NaCl and 0.987 for KCl, and (c) urKREEP with $\Delta^{37}$Cl of 25‰ (Boyce et al., 2018) and Na/K of 0.875 (Warren, 1989). The arrows in (b) and (c) represent the $^{41}$K enrichment ($\Delta^{41}$K >0.58‰) in urKREEP relative to mare basalt. The rectangle labeled as mare basalt represent the initial Na/K and Cl/K ratios in lunar melt, i.e., ratios in olivine-hosted melt inclusion (Ni et al., 2019). The rectangle and dashed line labeled as urKREEP represent the initial Na/K and Cl/K ratios and Cl isotopic fractionation factor in urKREEP (Warren, 1989; Boyce et al., 2018). The dashed line labeled as Earth represent the terrestrial Cl/K ratio (McDonough and Sun, 1995).

rate in the solid or the melt, has been experimentally investigated (Young et al., 1998; Wang et al., 1999; Richter et al., 2002; Sossi et al., 2020; Zhang et al., 2021). Typically, diffusion is the major homogenization process in solids. The ratio of the diffusion and the sublimation timescales $W$ can be used to assess the relative contributions of each process (Wang et al., 1999; Richter, 2004):

$$W = \frac{\tau_{diff}}{\tau_{sub}}, \tag{16}$$

where $\tau_{diff}$ is the diffusion timescale, and $\tau_{sub}$ is the sublimation timescale (see Supplementary Materials Section S2). The sublimating solid is homogeneous when $W < 1$ and has an isotopic gradient when $W \geq 1$ (Wang et al., 1999; Richter, 2004; Zhang et al., 2021).

A moving boundary 1-dimensional (1D) diffusion model (Wang et al., 1999) was used to numerically calculate the isotopic fractionation during sublimation (see Supplementary Materials Section S2). The numerical fits of the isotopic fractionation data suggest that in the sublimation experiments at $7\times10^{-5}$ bar, $W = 7\pm2$, whereas in the $10^{-2}$ bar experiments, $W$ ranged from 0 to 0.5 (Fig. S1). These calculations indicate that the sublimation rate was much higher than the diffusion rate in the solid at $7\times10^{-5}$ bar (Fig. 9a). The relatively small fractionation in the experiments at $7\times10^{-5}$ bar likely reflects diffusion-limited evaporation of the solid. Notably, the experimental samples with initial masses of 2 g were all sintered. This sintering may have affected the isotopic fractionation, resulting in the inability to quantitatively model the data for these samples (Fig. 3b). Overall, the isotopic fractionation in the diffusion-limited regime was likely significantly suppressed.

### 5.3. Mechanism of Cl and K isotope fractionation during KCl sublimation

The DFT calculations revealed that the $\alpha_{eq}$ of Cl between KCl gas and solid is very close to 1 (0.999989 at $T$=945 K; Balan et al., 2019). The similar bonding environment of K and Cl in the KCl gas and solid phases suggests that the $\alpha_{eq}$ of K can be assumed to be 1 at $T$>945 K in the present study. Therefore, similar to NaCl, the kinetic isotopic fractionation effect of KCl was much larger than its equilibrium isotopic fractionation effect as shown in Eq. (7). The saturation index $S$ of KCl was nearly the same as that of NaCl during sublimation (Table 3; Fig. 6a), indicating that the kinetic effect on the isotopic fractionation of KCl at the sublimation interface was very small. Similar to NaCl, the overall isotopic fractionation of KCl was controlled by mass transfer processes in both the gas and the solid.

The sublimation kinetics of KCl were similar to those of NaCl at each pressure (Fig. 6). As a result, the values of $^{37/35}$Cl($\alpha_{gas-solid}$) and $^{41/39}$K ($\alpha_{gas-solid}$) were similar to those obtained from the NaCl sublimation experiments (Fig. 7). The dimer ratio of sublimated KCl gas in our experiments was $26^{+17}_{-14}$ % at 945 K, close to 28% from our thermodynamic calculation (see Supplementary Materials Section S1; Chase 1988) and within the literature dimer ratio range of 14% to 27% (Miller and Kusch, 1956; Berkowitz and Chupka, 1958; Rothberg et al., 1959; Butman et al., 2000). Similarly, the value of $n$ obtained in our KCl sublimation experiments at $10^{-2}$ bar was ~ 1, and that at 1 bar was 0.4±0.1 (Fig. 8b), similar to the values obtained for NaCl. This similarity indicates that the sublimated KCl and NaCl gases experienced similar aerodynamic conditions. The timescale ratio between sublimation and diffusion in the solid during KCl sublimation was determined the same as that in NaCl (see Section 5.2.2). Similar to NaCl, the large $W$ value of 7±2 during KCl sublimation indicates that diffusion in the solid suppressed isotopic fractionation at $7\times10^{-5}$ bar (Fig. 9a).

The kinetic theory of gases predicts identical isotopic fractionation factors for K and Cl (Chapman and Cowling, 1970), but our experimental results have shown a correlation of potassium and chlorine isotopic fractionation with a slope of 0.82±0.06 (Fig. 4a). Similar deviations from theoretical predictions have been observed in the relationship between H and O isotopes during water vapor diffusion (Merlivat, 1978; Barkan and Luz, 2007; Luz et al., 2009). This deviation could be caused by thermal diffusion in the furnace, the effect of molecular collision diameters, and/or a flaw in the hard-sphere assumption in the kinetic theory of gases (Merlivat, 1978; Luz et al., 2009). Nevertheless, this minor systematic deviation in K and Cl isotopic fractionation does not affect our interpretation of the NaCl and KCl sublimation experiments.

In summary, pressure plays an important role in K and Cl isotopic fractionations, affecting convection in the gas phase and diffusion in the solid phase during sublimation of NaCl and KCl (Fig. 9b). Convection and advection with a turbulence factor $n$ of ~0.4 suppressed isotopic fractionation in the experiments performed at 1 bar. Chemical diffusion of sublimated gas was dominated by mass transfer in the sublimation experiments performed at <1 bar. The extremely fast sublimation of solid at $7\times10^{-5}$ bar led to diffusion-limited evaporation and isotope fractionation, and thus a deviation from 'ideal' kinetic isotope fractionation towards an effective α value closer to 1. It is reasonable to expect that the isotope fractionation factors of metals resulting from the evaporation of metal chlorides (e.g., $FeCl_2$ and $ZnCl_2$) could be similar to those of Cl.

### 5.4. Contribution of KCl degassing to K isotopic fractionation on the Moon

The sublimation experiments showed that KCl gas had similar isotopic fractionation factors for K and Cl. Chlorine isotopic fractionation can be used to evaluate the contribution of degassed KCl to K isotopic fractionation. This calculation requires mass fractions of all Cl-bearing species that result in Cl isotopic fractionation. Only NaCl and KCl were considered in these calculations. The mass fractions of NaCl and KCl in vapor were calculated using thermodynamic data with different Na/K molar fraction (Table S1) as the initial composition in the melt (see Supplementary Materials Section S3). Different Cl/K molar ratio (Table S1) was used as the initial ratio in the melt to evaluate the K loss during KCl degassing. Chlorine is a trace element in lunar silicate melt and thus the activities of NaCl and KCl ($a_{NaCl}$ and $a_{KCl}$) in the melt is $\ll 1$. Therefore, the $P_{Na_2Cl_2}/P_{NaCl}$ is close to zero using Eqs. (S6) and (7) (see Supplementary Materials Section S1). Only monomer was considered in all the following calculations. Free evaporation was firstly considered in the calculations to evaluate contribution of KCl degassing to K isotopic fractionation, with an isotopic fractionation factor of 0.9832 for NaCl and 0.9871 for KCl.

The largest isotopic fractionation ($\Delta^{37}Cl$) detected in different apatite grains within one lava sample is 15‰ from lunar samples (Tartèse et al., 2014; Treiman et al., 2014; Boyce et al., 2015; Barnes et al., 2016; Barnes et al., 2019; Ji et al., 2022), which are believed to be related to localized effects (Gargano et al., 2020). Using the chemical compositions of olivine-hosted melt inclusion in mare basalt, the melt Cl/K ratios range from 0.0035 to 0.015, and the Na/K ratios vary from 1.8 to 11.2 (Ni et al., 2019). These ranges of Cl/K and Na/K were used as the initial melt compositions in our calculations. The K isotopic fractionation induced by KCl vaporization from melts with 15‰ fractionation of Cl, expressed in $\Delta^{41}K$, is <0.1‰ (Fig. 10a). This small isotopic fractionation indicates that KCl degassing cannot significantly increase $\delta^{41}K$ in the melt during lava flow. We note that a transient atmosphere induced by magma degassing might have existed on the Moon (Needham and Kring, 2017; Hui et al., 2018; van Kooten et al., 2020). This atmosphere could lead to isotopic fractionation factors closer to unity for KCl and could even lower this estimation of the contribution to K isotope fractionation. Nevertheless, the small K isotope fractionation resulting from KCl evaporation estimated in this study is consistent with the limited variations in $\delta^{41}K$ (–0.07±0.09‰) that have thus far been reported for mare basalts (Tian et al., 2020).

Both K and Cl are incompatible and moderately volatile elements (Lodders., 2003), both of which were concentrated in urKREEP and may have undergone similar degassing during LMO solidification. The Cl isotopic composition of urKREEP is proposed to be 25‰ heavier than that of lunar mantle (Boyce et al., 2015; Barnes et al., 2016; Boyce et al., 2018). The $\delta^{41}K$ values of KREEP-bearing breccias are up to 0.51‰ (Tian et al., 2020). The fractionation of K isotopes between KREEP-bearing breccia and lunar basalt suggests that the K isotopic composition of urKREEP could be >0.58‰ heavier than that of lunar mantle. The Na/K of 0.9 and the Cl/K of 0.0031 ~ 0.0213 calculated for urKREEP (Table S1; Warren, 1989; Boyce et al., 2018) are assumed to be the initial compositions of the degassing melt. The isotope calculations similar to mare basalts show that KCl degassing can only introduce <0.2‰ of K isotope fractionation in urKREEP melt with 25‰ Cl isotope fractionation (Fig. 10b). By contrast, the Cl/K in undegassed (or less-degassed) urKREEP could be >0.0213. Assuming a higher initial Cl/K (e.g., 0.07 of BSE; McDonough and Sun, 1995) in urKREEP melt, 5% loss of K and 83% loss of Cl in this melt can lead to ~0.7‰ of K isotope fractionation (Fig. 10b). This K isotope fractionation is close to the largest K isotope composition in urKREEP, which is >0.58‰ heavier than that in lunar mantle. However, the assumption of free evaporation may overestimate the K isotopic fractionation in urKREEP melt because the actual Cl isotopic fractionation factor may be close to 1. Indeed, degassing of KCl in an urKREEP with $^{37/35}Cl(\alpha_{gas-melt})$ of 0.996–0.997 (Boyce et al., 2018), Na/K of 0.875 (Warren, 1989), and Cl/K of 0.07 (McDonough and Sun, 1995) can only produce ~0.2‰ K isotopic fractionation (Fig. 10c). Therefore, KCl degassing may not be the main contributor to the elevated K isotope composition in urKREEP. The Cl content has been believed to be lower than the K content in urKREEP (Table S1; Warren, 1989). Degassing of different K species is required to account for the heavy K isotope composition in urKREEP (Neuman et al., 2022). KCl may have been the main K-bearing species in the 270-bar steam atmospheres of Earth during magma ocean solidification (Fegley et al., 2016). However, degassing at such high pressure may be difficult to produce substantial isotopic fractionation for both K and Cl. Thermodynamic calculations have shown that $K^0$ is more abundant than KCl at lower pressure (Renggli et al., 2017; Sossi and Fegley, 2018). Furthermore, K isotopic fractionation might be larger at lower pressure (Richter et al., 2011). Therefore, degassing of $K^0$ may have been the main contributor to K isotope fractionation on the Moon with low Cl content. The isotope fractionations of Cl and K may have been decoupled during magma degassing on the Moon. However, KCl degassing of melt with elevated Cl/K may have facilitated K isotopic fractionation on the planetary bodies (Fig. 10).

### 5.5. Chlorine loss during lava flow on the Moon

The volatile coatings on lunar pyroclastic glass beads indicate that metal chlorides could have been released during volcanic eruptions on the Moon's surface (Butler and Meyer, 1976; McKay and Wentworth, 1993; Ma and Liu, 2019). Furthermore, the large variation of $\Delta^{37}Cl$ (5~15‰) in apatites from one mare basalt sample, which are also higher than that of the whole rock, likely reflects local degassing of flowing magma (Gargano et al., 2020). This chlorine loss during local degassing can be evaluated using the Cl isotopic fractionation factor determined in the present study. Assuming that lunar lava cooled in a 0.01-bar transient atmosphere consisting mainly of CO (Needham and Kring, 2017; Hui et al., 2018; Head et al., 2020; van Kooten et al, 2020), the saturation index of metal chlorides lost from the lava is close to unity using Eqs. (6) and (9). This estimation is based on the fact that the diffusion characteristic length $L$ in Eq. (9) of metal chloride from cooling lava on the Moon is much larger than that in our evaporation experiments where the saturation index was already close to 1. These assumptions imply that the isotopic fractionation factors of Cl degassing as NaCl and KCl from flowing lava in static CO gas at 0.01 bar on the Moon are 0.9946 and 0.9964 for NaCl and KCl, respectively, Using an isotopic fractionation factor of 0.9946, ≥94% loss of Cl in the lava might account for 15‰ $\Delta^{37}Cl$ variation in one sample. Convection in the transient atmosphere could have increased the Cl isotopic fractionation factor to unity and this would have required that more Cl degassed from the mare lava. However, the saturation index $S$ could become 0 if there was no atmosphere on the Moon. The Cl isotopic fractionation factors are 0.9832 during NaCl sublimation and 0.9871 for KCl on the airless Moon. Under these conditions, the variation of 15‰ $\Delta^{37}Cl$ in lunar basalt would require 58% to 68% of Cl degassing during lava flow.

### 5.6. Gas conditions for Cl isotope fractionation during the early stages of the Moon

Both lunar formation and the LMO could have resulted in the global Cl isotope fractionation shown in lunar samples. The whole-rock Cl isotope compositions of mare basalts show a relatively restricted variation with an average of 4.1±4.0‰ (Gargano et al., 2020). This average composition is proposed to be the Cl isotope composition (4.1±4.0‰) of the bulk Moon, the fractionation of which could have resulted from the giant impact (Gargano et al., 2020; Gargano et al., 2022). On the other hand, it has been proposed that urKREEP has heavy Cl isotope composition (25‰), a product of evaporation of the LMO (Boyce et al., 2018). Our experiments show that kinetic processes including diffusion in gas and evaporation in unsaturated gas media could induce isotope

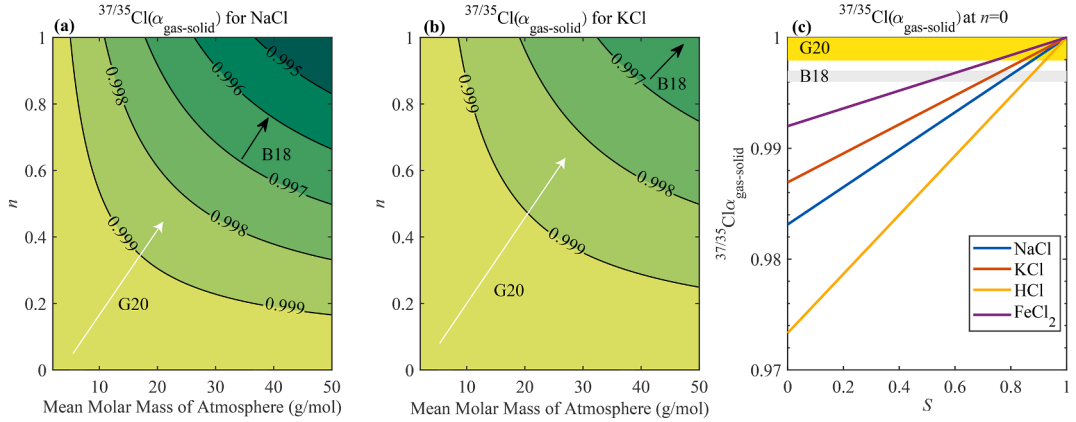


**Fig. 11.** Contour plot of $^{37/35}$Cl($\alpha_{gas–melt}$) for (a) NaCl and (b) KCl with average molar mass of atmosphere and turbulence factor. Saturation index $S = 1$ in all calculations. Black arrows (B18) represent the $^{37/35}$Cl($\alpha_{gas–melt}$) range of the LMO (Boyce et al., 2018). White arrows (G20) represent the range of $^{37/35}$Cl($\alpha_{gas–melt}$) during the giant impact (Gargano et al., 2020). (c) Correlation between $^{37/35}$Cl($\alpha_{gas–melt}$) and $S$ with $n = 0$. Gray bar (B18) represents the $^{37/35}$Cl($\alpha_{gas–melt}$) range of the LMO (Boyce et al., 2018). Yellow bar (G20) represents the range of $^{37/35}$Cl($\alpha_{gas–melt}$) during the giant impact (Gargano et al., 2020).

fractionation. Therefore, isotope fractionation factors could be used to evaluate the gas conditions in these two early stages of the Moon.

The bulk Moon $\Delta^{37}$Cl (4.1±4.0‰), together with the Cl content (0.39 ppm) of the Moon (Ni et al., 2019) and that (17 ppm) of the bulk silicate earth (McDonough and Sun, 1995), suggest that the Cl isotopic fractionation factor is $0.9989^{+0.0011}_{-0.0010}$ during the giant impact. This isotope fractionation factor indicates that evaporation process could have occurred during lunar formation. If this isotope fractionation was controlled by diffusion of NaCl and KCl in gas, the mean molar mass of this gas media was >10 g·mol$^{-1}$ and $n$ >0.2 (Fig. 11a, b). If this isotope fractionation was controlled by evaporation of NaCl and KCl in unsaturated gas media, the $S$ was <94% (Fig. 11c). These two scenarios indicate that the gas media was either relatively static or not very thick to produce such a large fractionation of Cl isotopes. These conditions are not consistent with the gas environment during the giant impact (Lock et al., 2018). Nevertheless, our experiments carried out at ≤1 bar may not be applicable to the conditions of giant impact.

The Cl isotopic fractionation factor (0.996–0.997) of the LMO (Boyce et al., 2018) is close to those determined for NaCl (0.9958) and KCl (0.9972) at $10^{-2}$ bar in the present study, as well as that determined for HCl (0.996) at 1 bar (Sharp et al., 2010a). These similarities suggest that a transient atmosphere may have existed above the LMO surface, in which the evaporated Cl as a mixture of NaCl, KCl, and HCl with $S$ close to 1 was transported with $n$>0.5 (Fig. 11a). The calculations indicate that the average molar mass of this atmosphere was >20 g·mol$^{-1}$. This molar mass is consistent with the molar mass of Na and SiO for the proposed composition of a Na-rich silicate-vapor atmosphere above the LMO (Visscher and Fegley, 2013; Saxena et al., 2017; Charnoz et al., 2021). However, this estimation is different from the molar mass of lunar atmosphere estimated using evaporation of Cu, Zn, Rb, and K (Sossi et al., 2020). This difference may result from different model settings. Furthermore, the turbulence factor $n$> 0.5 requires the atmosphere above the LMO to have been relatively static.

The large heat gradient over the LMO could have induced vigorous convection and prevented a chemical gradient in the atmosphere (Thompson and Stevenson, 1988; Saxena et al., 2017), resulting in $n$=0 and $\alpha_{tran}$=1. In that case, no isotopic fractionation would have occurred during LMO crystallization if the evaporation interface was near equilibrium (Tang and Young, 2020). However, the tide pull from Earth could have promoted the hydrodynamic escape of atmosphere above the LMO and resulted in a decrease of the saturation index to <1 at the LMO surface (Charnoz et al., 2021). Nevertheless, the large Cl isotopic fractionation in KREEP requires that $S$ <0.85 at the interface even with HCl (the Cl-bearing species with the lowest mass) as the evaporation species (Fig. 11c). This small $S$ indicates that the atmosphere above the LMO may not have been very thick.

## 6. Conclusion

We performed NaCl and KCl sublimation experiments at three different pressures and measured K and Cl isotope compositions in the experimental residues. The $^{37/35}$Cl($\alpha_{gas–solid}$) values determined in our NaCl experiments were 0.9985±0.0002 at 1 bar, 0.9958±0.0004 at $10^{-2}$ bar, and 0.99807±0.00004 at $7\times10^{-5}$ bar. The $^{41/39}$K($\alpha_{gas–solid}$) and $^{37/35}$Cl($\alpha_{gas–solid}$) values determined in our KCl experiments were 0.99884 ±0.00004 and 0.9988±0.0003 at 1 bar, 0.9977±0.0002 and 0.9972 ±0.0003 at $10^{-2}$ bar, and 0.9989±0.0002 and 0.9989±0.0001 at $7\times10^{-5}$ bar, respectively. The Cl and K isotopic fractionations were greater at $10^{-2}$ bar than those at $7\times10^{-5}$ bar and at 1 bar for both NaCl and KCl. The large saturation index (>95 %) for all of the experiments indicates near equilibrium at the sublimation interface. The isotopic fractionations at $10^{-2}$ bar were controlled by the chemical diffusion of sublimated gas in mass transfer, yielding dimer ratios for NaCl and KCl of $20^{+8}_{-7}$ % and $26^{+17}_{-14}$ %, respectively. Convection in gas mass transfer at 1 bar with a turbulence factor of 0.4±0.1 suppressed isotopic fractionation. The sublimation rate was much larger than the homogenization rate in the solid at $7\times10^{-5}$ bar, which suppressed isotopic fractionation. KCl degassing contributed little to K isotopic fractionation using Cl/K and Na/K in the lunar melt, indicating that K isotopic compositions in lunar samples were likely unaffected by degassing of KCl. By contrast, 15‰ of $\Delta^{37}$Cl variation in the lunar basalt samples can be explained by >58% of Cl degassed as metal chlorides during lava flow on the Moon. Our $^{37/35}$Cl($\alpha_{gas–melt}$) results are close to the published isotopic fractionation factor of Cl from the LMO ($\alpha$ =0.996~0.997; Boyce et al., 2018), indicating that Cl might have fractionated in an atmosphere above the LMO.

## Declaration of Competing Interest

The authors declare that they have no known competing financial interests or personal relationships that could have appeared to influence the work reported in this paper.

*Acknowledgements*

This research was supported by National Natural Science Foundation of China (NSFC) grant (42125303), B-type Strategic Priority Program of the Chinese Academy of Sciences (XDB41000000), and China National

Space Administration (CNSA) grant (D020205). We thank editor Dr. James Day for efficiently handling our manuscript, and Dr. Paolo Sossi and two anonymous reviewers for constructive and detailed comments. Z.H. is grateful to assistance of Dr. Yibo Lin and Dr. Xi Liu on TIMS, Dr. Shichao An on MC-ICP-MS, Dr. Xi Liu, Yijing Wang and Zhiguang Xia on sample preparation, Dr. Sheng Shang and Ge Dong on high temperature furnace, Xianglong Luo on flame photometer, and Kang Shuai, Dr. Haolan Tang and Dr. Jessica Barnes for insightful discussion.

*Data availability*

The data supporting the findings of this study are available within the article and Supplementary Material.

## Appendix A. Supplementary material

Supplementary material associated with this article can be found in the online version. It includes the details on how to calculate isotope fractionation factor of mixed species, diffusion in the solid and NaCl/KCl ratio in gas. A summary of mass ratios of Na/K and Cl/K used for the calculations and an additional figure showing effect of diffusion in the solid on isotope fractionation are also included in the supplementary material.

Supplementary material to this article can be found online at https://doi.org/10.1016/j.gca.2023.05.007.

## References

Albarède, F., Albalat, E., Lee, C.-T.-A., 2015. An intrinsic volatility scale relevant to the Earth and Moon and the status of water in the Moon. Meteorit. Planet. Sci. 50, 568–577.

An, S., Luo, X., Li, W., 2022. Precise measurement of $^{41}K/^{39}K$ ratios by high-resolution multicollector inductively coupled plasma mass spectrometry under a dry and hot plasma setting. Rapid Commun. Mass Spectrom. 36, e9289.

Balan, E., Créon, L., Sanloup, C., Aléon, J., Blanchard, M., Paulatto, L., Bureau, H., 2019. First-principles modeling of chlorine isotope fractionation between chloride-bearing molecules and minerals. Chem. Geol. 525, 424–434.

Barkan, E., Luz, B., 2007. Diffusivity fractionations of $H_2^{16}O/H_2^{17}O$ and $H_2^{16}O/H_2^{18}O$ in air and their implications for isotope hydrology. Rapid Commun. Mass Spectrom. 21, 2999–3005.

Barnes, J.J., Tartèse, R., Anand, M., McCubbin, F.M., Neal, C.R., Franchi, I.A., 2016. Early degassing of lunar urKREEP by crust-breaching impact(s). Earth Planet. Sci. Lett. 447, 84–94.

Barnes, J.J., Franchi, I.A., McCubbin, F.M., Anand, M., 2019. Multiple reservoirs of volatiles in the Moon revealed by the isotopic composition of chlorine in lunar basalts. Geochim. Cosmochim. Acta 266, 144–162.

Barrett, T.J., Barnes, J.J., Anand, M., Franchi, I.A., Greenwood, R.C., Charlier, B.L.A., Zhao, X., Moynier, F., Grady, M.M., 2019. Investigating magmatic processes in the early Solar System using the Cl isotopic systematics of eucrites. Geochim. Cosmochim. Acta 266, 582–597.

Bartlett, R.W., 1967. Platinum oxidation kinetics with corrective diffusion and surface reaction. J. Electrochem. Soc. 114, 547–550.

Bellucci, J.J., Whitehouse, M.J., John, T., Nemchin, A.A., Snape, J.F., Bland, P.A., Benedix, G.K., 2017. Halogen and Cl isotopic systematics in Martian phosphates: Implications for the Cl cycle and surface halogen reservoirs on Mars. Earth Planet. Sci. Lett. 458, 192–202.

Berkowitz, J., Chupka, W.A., 1958. Polymeric gaseous molecules in the vaporization of alkali halides. J. Chem. Phys. 29, 653–657.

Boyce, J.W., Treiman, A.H., Guan, Y., Ma, C., Eiler, J.M., Gross, J., Greenwood, J.P., Stolper, E.M., 2015. The chlorine isotope fingerprint of the lunar magma ocean. Sci. Adv. 1, e1500380.

Boyce, J.W., Kanee, S.A., McCubbin, F.M., Barnes, J.J., Bricker, H., Treiman, A.H., 2018. Early loss, fractionation, and redistribution of chlorine in the Moon as revealed by the low-Ti lunar mare basalt suite. Earth Planet. Sci. Lett. 500, 205–214.

Butler, P., Meyer, C., 1976. Sulfur prevails in coatings on glass droplets: Apollo 15 green and brown glasses and Apollo 17 orange and black (devitrified) glasses. Proc. Lunar Sci. Conf. 7, 1561–1581.

Butman, M.F., Smirnov, A.A., Kudin, L.S., Munir, Z.A., 2000. Mass-spectrometric study of the temperature variation in the dimer-to-monomer ratio in the free-surface vaporization fluxes from alkali halide crystals. J. Mater. Synth. Process. 8, 93–100.

Cappa, C.D., 2003. Isotopic fractionation of water during evaporation. J. Geophys. Res. 108, 4525.

Chapman, S., Cowling, T. G., 1970. The Mathematical Theory of Non-uniform Gases., Cambridge University Press, Cambridge.

Charnoz, S., Sossi, P.A., Lee, Y.-N., Siebert, J., Hyodo, R., Allibert, L., Pignatale, F.C., Landeau, M., Oza, A.V., Moynier, F., 2021. Tidal pull of the Earth strips the proto-Moon of its volatiles. Icarus 364, 114451.

Chase, M. W., 1998. NIST-JANAF Thermochemical Tables, 4th Ed. J. Phys. Chem. Ref. Data, Monograph 9 (Part I and Part II). Am. Inst. Phys.

Craig, H., Gordon, L.I., Horibe, Y., 1963. Isotopic exchange effects in the evaporation of water: 1. Low-temperature experimental results. J. Geophys. Res. 68, 5079–5087.

Dauphas, N., Janney, P.E., Mendybaev, R.A., Wadhwa, M., Richter, F.M., Davis, A.M., Van Zuilen, M., Hines, R., Foley, C.N., 2004. Chromatographic separation and multicollection-ICPMS analysis of iron. Investigating mass-dependent and -independent isotope effects. Anal. Chem. 76, 5855–5863.

Davis, A.M., Hashimoto, A., Clayton, R.N., Mayeda, T.K., 1990. Isotope mass fractionation during evaporation of $Mg_2SiO_4$. Nature 347, 655–658.

Day, J.M.D., Moynier, F., 2014. Evaporative fractionation of volatile stable isotopes and their bearing on the origin of the Moon. Philos. Trans. R. Soc. A Math. Phys. Eng. Sci. 372, 20130259.

De Maria, G., Balducci, G., Guido, M., Piacente, V., 1971. Mass spectrometric investigation of the vaporization process of Apollo 12 lunar samples. Proc. Lunar Sci. Conf. 2, 1367–1380.

Dhaliwal, J.K., Day, J.M.D., Moynier, F., 2018. Volatile element loss during planetary magma ocean phases. Icarus 300, 249–260.

Ewing, C.T., Stern, K.H., 1973. Vaporization kinetics of sodium chloride. I. The solid. J. Phys. Chem. 77, 1442–1449.

Ewing, C.T., Stern, K.H., 1974. Equilibrium vaporization rates and vapor pressures of solid and liquid sodium chloride, potassium chloride, potassium bromide, cesium iodide, and lithium fluoride. J. Phys. Chem. 78, 1998–2005.

Fegley, B., Jacobson, N.S., Williams, K.B., Plane, J.M.C., Schaefer, L., Lodders, K., 2016. Solubility of rock in steam atmospheres of planets. Astrophys. J. 824, 103.

Gargano, A., Sharp, Z., Shearer, C., Simon, J.I., Halliday, A., Buckley, W., 2020. The Cl isotope composition and halogen contents of Apollo-return samples. Proc. Natl. Acad. Sci. U. S. A. 117, 23418–23425.

Gargano, A., Dottion, J., Hopkins, S.S., Sharp, Z., Shearer, C., Halliday, A., Larner, F., Farquar, J., Simon, J., 2022. The Zn, S, and Cl isotope compositions of mare basalts: Implications for the effects of eruption style and pressure on volatile element stable isotope fractionation on the Moon. Am. Mineral. 107, 1985–1994.

Gargano, A., Sharp, Z., 2019. The chlorine isotope composition of iron meteorites: Evidence for the Cl isotope composition of the solar nebula and implications for extensive devolatilization during planet formation. Meteorit. Planet. Sci. 54, 1619–1631.

Gonfiantini, R., Wassenaar, L.I., Araguas-Araguas, L., Aggarwal, P.K., 2018. A unified Craig-Gordon isotope model of stable hydrogen and oxygen isotope fractionation during fresh or saltwater evaporation. Geochim. Cosmochim. Acta 235, 224–236.

Hashimoto, A., 1990. Evaporation kinetics of forsterite and implications for the early solar nebula. Nature 347, 53–55.

Head, J.W., Wilson, L., Deutsch, A.N., Rutherford, M.J., Saal, A.E., 2020. Volcanically induced transient atmospheres on the Moon: Assessment of duration, significance, and contributions to polar volatile traps. Geophys. Res. Lett. 47 e2020GL089509.

Herzog, G.F., Moynier, F., Albarède, F., Berezhnoy, A.A., 2009. Isotopic and elemental abundances of copper and zinc in lunar samples, Zagami, Pele's hairs, and a terrestrial basalt. Geochim. Cosmochim. Acta 73, 5884–5904.

Hirth, J.P., Pound, G.M., 1963. Condensation and Evaporation: Nucleation and Growth Kinetics. MacMillan, New York.

Horita, J., Rozanski, K., Cohen, S., 2008. Isotope effects in the evaporation of water: A status report of the Craig-Gordon model. Isotopes Environ. Health Stud. 44, 23–49.

Hu, S., Lin, Y., Anand, M., Franchi, I.A., Zhao, X., Zhang, J., Hao, J., Zhang, T., Yang, W., Changela, H., 2020. Deuterium and $^{37}$chlorine rich fluids on the surface of Mars: Evidence from the enriched basaltic shergottite Northwest Africa 8657. J. Geophys. Res. Planets 125 e2020JE006537.

Hui, H., Hess, K.U., Zhang, Y., Nichols, A.R.L., Peslier, A.H., Lange, R.A., Dingwell, D.B., Neal, C.R., 2018. Cooling rates of lunar orange glass beads. Earth Planet. Sci. Lett. 503, 88–94.

Jacobson, N.S., Kuczmarski, M.A., Kowalski, B.A., 2020. Vaporization of protective oxide films into different gas atmospheres. Oxid. Met. 93, 247–282.

Ji, J., He, H., Hu, S., Lin, Y., Hui, H., Hao, J., Li, R., Yang, W., Yan, Y., Tian, H., Zhang, C., Anand, M., Tartèse, R., Gu, L., Li, J., Zhang, D., Mao, Q., Jia, L., Chen, Y., Wu, S., Wang, H., He, H., Li, X., Wu, F., 2022. Magmatic chlorine isotope fractionation recorded in apatite from Chang'e-5 basalts. Earth Planet. Sci. Lett. 591, 117636.

Kato, C., Moynier, F., Valdes, M.C., Dhaliwal, J.K., Day, J.M.D., 2015. Extensive volatile loss during formation and differentiation of the Moon. Nat. Commun. 6, 1–4.

Klemme, S., Genske, F., Sossi, P.A., Berndt, J., Renggli, C.J., Stracke, A., 2022. Cr stable isotope fractionation by evaporation from silicate melts. Chem. Geol. 121096.

Kvande, H., Linga, H., Motzfeldt, K., Wahlbeck, P.G., Hoyer, E., Spiridonov, V.P., Strand, T.G., 1979. A thermogravimetric method for determination of vapour pressures above $10^{-2}$ atm. II. Vapour pressure of molten sodium chloride. Acta Chem. Scand. A 33, 281–288.

Lester, J.E., Somorjai, G.A., 1968. Studies of the evaporation mechanism of sodium chloride single crystals. J. Chem. Phys. 49, 2940–2949.

Lock, S.J., Stewart, S.T., Petaev, M.I., Leinhardt, Z., Mace, M.T., Jacobsen, S.B., Cuk, M., 2018. The origin of the Moon within a terrestrial synestia. J. Geophys. Res. Planets 123, 910–951.

Lodders, K., 2003. Solar system abundances and condensation temperatures of the elements. Astrophys. J. 591, 1220–1247.

Luz, B., Barkan, E., Yam, R., Shemesh, A., 2009. Fractionation of oxygen and hydrogen isotopes in evaporating water. Geochim. Cosmochim. Acta 73, 6697–6703.

Ma, C., Liu, Y., 2019. Discovery of a zinc-rich mineral on the surface of lunar orange pyroclastic beads. Am. Mineral. 104, 447–452.

McDonough, W.F., Sun, S.S., 1995. The composition of the Earth. Chem. Geol. 120, 223–253.

McKay, D.S., Wentworth, S.J., 1993. Grain surface features of Apollo 17 orange and black glass. Proc. Lunar Planet. Sci. Conf. 24, 961–962.
Mendybaev, R.A., Richter, F.M., Georg, R.B., Janney, P.E., Spicuzza, M.J., Davis, A.M., Valley, J.W., 2013. Experimental evaporation of Mg- and Si-rich melts: Implications for the origin and evolution of FUN CAIs. Geochim. Cosmochim. Acta 123, 368–384.
Merlivat, L., 1978. Molecular diffusivities of $H_2^{16}O$, $HD^{16}O$, and $H_2^{18}O$ in gases. J. Chem. Phys. 69, 2864.
Miller, R.C., Kusch, P., 1956. Molecular composition of alkali halide vapors. J. Chem. Phys. 25, 860–876.
Milne, T.A., Klein, H.M., 1960. Mass spectrometric study of heats of dimerization of alkali chlorides. J. Chem. Phys. 33, 1628–1637.
Needham, D.H., Kring, D.A., 2017. Lunar volcanism produced a transient atmosphere around the ancient Moon. Earth Planet. Sci. Lett. 478, 175–178.
Neuman, M., Holzheid, A., Lodders, K., Fegley, B., Jolliff, B.L., Koefoed, P., Chen, H., Wang, K., 2022. High temperature evaporation and isotopic fractionation of K and Cu. Geochim. Cosmochim. Acta 316, 1–20.
Ni, P., Zhang, Y., Chen, S., Gagnon, J., 2019. A melt inclusion study on volatile abundances in the lunar mantle. Geochim. Cosmochim. Acta 249, 17–41.
Nie, N.X., Dauphas, N., 2019. Vapor drainage in the protolunar disk as the cause for the depletion in volatile elements of the Moon. Astrophys. J. 884, L48.
Nielsen, S.G., Shu, Y., Wood, B.J., Blusztajn, J., Auro, M., Norris, C.A., Wörner, G., 2021. Thallium isotope fractionation during magma degassing: Evidence from experiments and Kamchatka arc lavas. Geochem. Geophys. Geosys. 22, 1–15.
O'Neill, H.S.C., 1991. The origin of the Moon and the early history of the Earth—A chemical model. Part 1: The Moon. Geochim. Cosmochim. Acta 55, 1135–1157.
Palme, H., Larimer, J.W., Lipschutz, M.E., 1988. Moderately volatile elements. In: Meteorites and the Early Solar System. University of Arizona Press, pp. 436–461.
Paniello, R.C., Day, J.M.D., Moynier, F., 2012. Zinc isotopic evidence for the origin of the Moon. Nature 490, 376–379.
Potts, N.J., Barnes, J.J., Tartèse, R., Franchi, I.A., Anand, M., 2018. Chlorine isotopic compositions of apatite in Apollo 14 rocks: Evidence for widespread vapor-phase metasomatism on the lunar nearside ~4 billion years ago. Geochim. Cosmochim. Acta 230, 46–59.
Pringle, E.A., Moynier, F., 2017. Rubidium isotopic composition of the Earth, meteorites, and the Moon: Evidence for the origin of volatile loss during planetary accretion. Earth Planet. Sci. Lett. 473, 62–70.
Renggli, C.J., King, P.L., Henley, R.W., Norman, M.D., 2017. Volcanic gas composition, metal dispersion and deposition during explosive volcanic eruptions on the Moon. Geochim. Cosmochim. Acta 206, 296–311.
Renggli, C.J., Hellmann, J.L., Burkhardt, C., Klemme, S., Berndt, J., Pangritz, P., Kleine, T., 2022. Tellurium isotope fractionation during evaporation from silicate melts. Geochim. Cosmochim. Acta 339, 35–45.
Richter, F.M., 2004. Timescales determining the degree of kinetic isotope fractionation by evaporation and condensation. Geochim. Cosmochim. Acta 68, 4971–4992.
Richter, F.M., Davis, A.M., Ebel, D.S., Hashimoto, A., 2002. Elemental and isotopic fractionation of Type B calcium-, aluminum-rich inclusions: Experiments, theoretical considerations, and constraints on their thermal evolution. Geochim. Cosmochim. Acta 66, 521–540.
Richter, F.M., Janney, P.E., Mendybaev, R.A., Davis, A.M., Wadhwa, M., 2007. Elemental and isotopic fractionation of Type B CAI-like liquids by evaporation. Geochim. Cosmochim. Acta 71, 5544–5564.
Richter, F.M., Mendybaev, R.A., Christensen, J.N., Ebel, D., Gaffney, A., 2011. Laboratory experiments bearing on the origin and evolution of olivine-rich chondrules. Meteorit. Planet. Sci. 46, 1152–1178.
Rodríguez, A., van Bergen, M.J., Eggenkamp, H.G.M., 2018. Experimental evaporation of hyperacid brines: Effects on chemical composition and chlorine isotope fractionation. Geochim. Cosmochim. Acta 222, 467–484.
Rothberg, G.M., Eisenstadt, M., Kusch, P., 1959. Free evaporation of alkali halide crystals. J. Chem. Phys. 30, 517–527.
Sata, T., 1992. Vaporization rates from sintered bodies and single crystals of NaCl in flowing air. J. Mater. Sci. 27, 2946–2951.
Saxena, P., Elkins-Tanton, L., Petro, N., Mandell, A., 2017. A model of the primordial lunar atmosphere. Earth Planet. Sci. Lett. 474, 198–205.
Scholtysik, R., Canil, D., 2021. The effects of S, Cl and oxygen fugacity on the sublimation of volatile trace metals degassed from silicate melts with implications for volcanic emissions. Geochim. Cosmochim. Acta 301, 141–157.
Sharp, Z.D., Barnes, J.D., Fischer, T.P., Halick, M., 2010a. An experimental determination of chlorine isotope fractionation in acid systems and applications to volcanic fumaroles. Geochim. Cosmochim. Acta 74, 264–273.
Sharp, Z.D., Shearer, C.K., McKeegan, K.D., Barnes, J.D., Wang, Y.Q., 2010b. The chlorine isotope composition of the Moon and implications for an anhydrous mantle. Science 329, 1050–1053.
Sharp, Z.D., McCubbin, F.M., Shearer, C.K., 2013a. A hydrogen-based oxidation mechanism relevant to planetary formation. Earth Planet. Sci. Lett. 380, 88–97.
Sharp, Z.D., Mercer, J.A., Jones, R.H., Brearley, A.J., Selverstone, J., Bekker, A., Stachel, T., 2013b. The chlorine isotope composition of chondrites and Earth. Geochim. Cosmochim. Acta 107, 189–204.
Sossi, P.A., Fegley, B., 2018. Thermodynamics of element volatility and its application to planetary processes. Rev. Mineral. Geochemistry 84, 393–460.
Sossi, P.A., Moynier, F., Van Zuilen, K., 2018. Volatile loss following cooling and accretion of the Moon revealed by chromium isotopes. Proc. Natl. Acad. Sci. U. S. A. 115, 10920–10925.
Sossi, P.A., Klemme, S., O'Neill, H.S.C., Berndt, J., Moynier, F., 2019. Evaporation of moderately volatile elements from silicate melts: Experiments and theory. Geochim. Cosmochim. Acta 260, 204–231.
Sossi, P.A., Moynier, F., Treilles, R., Mokhtari, M., Wang, X., Siebert, J., 2020. An experimentally-determined general formalism for evaporation and isotope fractionation of Cu and Zn from silicate melts between 1300 and 1500 °C and 1 bar. Geochim. Cosmochim. Acta 288, 316–340.
Stewart, M.K., 1975. Stable isotope fractionation due to evaporation and isotopic exchange of falling waterdrops: Applications to atmospheric processes and evaporation of lakes. J. Geophys. Res. 80, 1133–1146.
Symonds, R.B., Reed, M.H., 1993. Calculation of multicomponent chemical equilibria in gas-solid-liquid systems: Calculation methods, thermochemical data, and applications to studies of high-temperature volcanic gases with examples from Mount St. Helens. Am. J. Sci. 293, 758–864.
Tang, H., Young, E.D., 2020. Evaporation from the lunar magma ocean was not the mechanism for fractionation of the Moon's moderately volatile elements. Planet. Sci. J. 1, 49.
Tartèse, R., Anand, M., Joy, K.H., Franchi, I.A., 2014. H and Cl isotope systematics of apatite in brecciated lunar meteorites Northwest Africa 4472, Northwest Africa 773, Sayh al Uhaymir 169, and Kalahari 009. Meteorit. Planet. Sci. 49, 2266–2289.
Thompson, C., Stevenson, D.J., 1988. Gravitational instability in two-phase disks and the origin of the Moon. Astrophys. J. 333, 452.
Tian, Z., Jolliff, B.L., Korotev, R.L., Fegley, B., Lodders, K., Day, J.M.D., Chen, H., Wang, K., 2020. Potassium isotopic composition of the Moon. Geochim. Cosmochim. Acta 280, 263–280.
Treiman, A.H., Boyce, J.W., Gross, J., Guan, Y., Eiler, J.M., Stolper, E.M., 2014. Phosphate-halogen metasomatism of lunar granulite 79215: Impact-induced fractionation of volatiles and incompatible elements. Am. Mineral. 99, 1860–1870.
Ustunisik, G., Nekvasil, H., Lindsley, D.H., McCubbin, F.M., 2015. Degassing pathways of Cl-, F-, H-, and S-bearing magmas near the lunar surface: Implications for the composition and Cl isotopic values of lunar apatite. Am. Mineral. 100, 1717–1727.
van Kooten, E.M.M.E., Moynier, F., Day, J.M.D., 2020. Evidence for transient atmospheres during eruptive outgassing on the Moon. Planet. Sci. J. 1, 67.
Visscher, C., Fegley, B., 2013. Chemistry of impact-generated silicate melt-vapor debris disks. Astrophys. J. Lett. 767, 12.
Wagoner, R.H., Hirth, J.P., 1977. Vaporization kinetics of sodium chloride. J. Chem. Phys. 67, 3074–3083.
Wang, J., Davis, A.M., Clayton, R.N., Hashimoto, A., 1999. Evaporation of single crystal forsterite: Evaporation kinetics, magnesium isotope fractionation, and implications of mass-dependent isotopic fractionation of a diffusion-controlled reservoir. Geochim. Cosmochim. Acta 63, 953–966.
Wang, X., Fitoussi, C., Bourdon, B., Fegley, B., Charnoz, S., 2019a. Tin isotopes indicative of liquid-vapour equilibration and separation in the Moon-forming disk. Nat. Geosci. 12, 707–711.
Wang, Y., Hsu, W., Guan, Y., 2019b. An extremely heavy chlorine reservoir in the Moon: Insights from the apatite in lunar meteorites. Sci. Rep. 9, 5727.
Wang, K., Jacobsen, S.B., 2016. Potassium isotopic evidence for a high-energy giant impact origin of the Moon. Nature 538, 487–490.
Warren, P. H., 1989. KREEP: Major-element diversity, trace-element uniformity (almost). In Workshop on Moon in Transition: Apollo 14, KREEP, and Evolved Lunar Rocks pp. 149–153.
Wei, H.Z., Jiang, S.Y., Xiao, Y.K., Wang, J., Lu, H., Wu, B., Wu, H.P., Li, Q., Luo, C.G., 2012. Precise determination of the absolute isotopic abundance ratio and the atomic weight of chlorine in three international reference materials by the positive thermal ionization mass spectrometer-$Cs_2Cl^+$-graphite method. Anal. Chem. 84, 10350–10358.
Williams, J.T., Shearer, C.K., Sharp, Z.D., Burger, P.V., McCubbin, F.M., Santos, A.R., Agee, C.B., McKeegan, K.D., 2016. The chlorine isotopic composition of Martian meteorites 1: Chlorine isotope composition of Martian mantle and crustal reservoirs and their interactions. Meteorit. Planet. Sci. 51, 2092–2110.
Wimpenny, J., Borg, L., Sio, C.K.I., 2022. The gallium isotopic composition of the Moon. Earth Planet. Sci. Lett. 578, 117318.
Xiao, Y.K., Zhang, C.G., 1992. High precision isotopic measurement of chlorine by thermal ionization mass spectrometry of the $Cs_2Cl^+$ ion. Int. J. Mass Spectrom. Ion Process. 116, 183–192.
Xiao, Y.K., Zhou, Y., Wang, Q., Wei, H., Liu, W., Eastoe, C.J., 2002. A secondary isotopic reference material of chlorine from selected seawater. Chem. Geol. 182, 655–661.
Young, E.D., Nagahara, H., Mysen, B.O., Audet, D.M., 1998. Non-Rayleigh oxygen isotope fractionation by mineral evaporation: Theory and experiments in the system $SiO_2$. Geochim. Cosmochim. Acta 62, 3109–3116.
Young, E.D., Shahar, A., Nimmo, F., Schlichting, H.E., Schauble, E.A., Tang, H., Labidi, J., 2019. Near-equilibrium isotope fractionation during planetesimal evaporation. Icarus 323, 1–15.
Young, E.D., Macris, C.A., Tang, H., Hogan, A.A., Shollenberger, Q.R., 2022. Isotope velocimetry: Experimental and theoretical demonstration of the potential importance of gas flow for isotope fractionation during evaporation of protoplanetary material. Earth Planet. Sci. Lett. 589, 117575.
Yu, Y., Hewins, R.H., Alexander, C.M.O.D., Wang, J., 2003. Experimental study of evaporation and isotopic mass fractionation of potassium in silicate melts. Geochim. Cosmochim. Acta 67, 773–786.
Zhang, Y., 2020. $H_2O$ and other volatiles in the Moon, 50 years and on. ACS Earth Sp. Chem. 4, 1480–1499.
Zhang, Z.J., Nie, N.X., Mendybaev, R.A., Liu, M., Hu, J.J., Hopp, T., Alp, E.E., Lavina, B., Bullock, E.S., McKeegan, K.D., Dauphas, N., 2021. Loss and isotopic fractionation of

alkali elements during diffusion-limited evaporation from molten silicate: Theory and experiments. ACS Earth Sp. Chem. 5, 755–784.
Zhang, W., Oganov, A.R., Goncharov, A.F., Zhu, Q., Boulfelfel, S.E., Lyakhov, A.O., Stavrou, E., Somayazulu, M., Prakapenka, V.B., Konôpková, Z., 2013. Unexpected stable stoichiometries of sodium chlorides. Science 342, 1502–1505.
Zimm, B.H., Mayer, J.E., 1944. Vapor pressures, heats of vaporization, and entropies of some alkali halides. J. Chem. Phys. 12, 362–369.